Development of a Spectroscopic Technique for Continuous Online Monitoring of Oxygen and Site-Specific Nitrogen Isotopic Composition of Atmospheric Nitrous Oxide

Citation: Harris, Eliza, David D. Nelson, William Olszewski, Mark Zahniser, Katherine E. Potter, Barry J. McManus, Andrew Whitehill, Ronald G. Prinn, and Shuhei Ono. "Development of a Spectroscopic Technique for Continuous Online Monitoring of Oxygen and Site-Specific Nitrogen Isotopic Composition of Atmospheric Nitrous Oxide." Analytical Chemistry 86, no. 3 (February 4, 2014): 1726–1734.

As Published: http://dx.doi.org/10.1021/ac403606u

Publisher: American Chemical Society (ACS)

Persistent URL: http://hdl.handle.net/1721.1/92437

Version: Author's final manuscript: final author's manuscript post peer review, without publisher's formatting or copy editing

Development of a spectroscopic technique for continuous online monitoring of oxygen and site-specific nitrogen isotopic composition of atmospheric nitrous oxide

Eliza Harris,*,†,‡ David D. Nelson,¶ William Olsewski,† Mark Zahniser,¶ Katherine E. Potter,† Barry J. McManus,¶ Andrew Whitehill,† Ronald G. Prinn,† and Shuhei Ono†

Department of Earth, Atmospheric and Planetary Sciences, Massachusetts Institute of Technology, 77 Massachusetts Ave, 02139 Cambridge USA, Laboratory for Air Pollution and Environmental Technology, Swiss Federal Institute for Materials Science and Technology (EMPA), Überlandstrasse 129, 8600 Dübendorf Switzerland, and Atmospheric and Environmental Chemistry, Aerodyne Research Inc., 45 Manning Road, 01821 Billerica USA

E-mail: elizah@mit.edu

Abstract

Nitrous oxide is an important greenhouse gas and ozone depleting-substance. Its sources are diffuse and poorly characterised, complicating efforts to understand anthropogenic impacts and develop mitigation policies. Online, spectroscopic analysis of N_2O isotopic composition

*To whom correspondence should be addressed
†Massachusetts Institute of Technology
‡Now at: Swiss Federal Laboratories for Materials Science and Technology
¶Aerodyne Research

can provide continuous measurements at high time resolution, giving new insight into N_2O sources, sinks and chemistry. We present a new preconcentration unit, 'Stheno II', coupled to a tunable infrared laser direct absorption spectroscopy (TILDAS) instrument, to measure ambient-level variations in ^{18}O and site-specific ^{15}N N_2O isotopic composition at remote sites with a temporal resolution of $<$1 hour.

Trapping of N_2O is quantitative up to a sample size of $\sim$4 L, with an optimal sample size of 1200-1800 mL at a sampling frequency of 28 minutes. Line shape variations with the partial pressure of the major matrix gases N_2/O_2 and CO_2 are measured, and show that characterisation of both pressure broadening and Dicke narrowing is necessary for an optimal spectral fit. Partial pressure variations of CO_2 and bath gas result in an linear isotopic measurement offset of 2.6-6.0 ‰ $mbar^{-1}$. Comparison of IR MS and TILDAS measurements shows that the TILDAS technique is accurate and precise, and less susceptible to interferences than IR MS measurements. Two weeks of measurements of N_2O isotopic composition from Cambridge, MA, in May 2013 are presented. The measurements show significant short-term variability in N_2O isotopic composition larger than the measurement precision, in response to meteorological parameters such as atmospheric pressure and temperature.

1 Introduction

Nitrous oxide (N_2O) is a potent, long-lived greenhouse gas[1] and, as a source of reactive nitrogen to the stratosphere, the dominant contributor to catalytic ozone destruction in the 21st century.[2] Since preindustrial times, N_2O mixing ratio in the troposphere has increased from 270 ppb to the current level of 324.2$\pm$0.1 ppb (2011) with an average growth rate of 0.2-0.3 % yr^{-1} over the past decades.[3–5] This increase has been attributed to anthropogenic perturbation of the nitrogen cycle, in particular the application of inorganic fertilisers.[5–8] The N_2O budget, however, is poorly constrained due to the high spatial and temporal variability of fluxes, which limits our ability to develop targeted mitigation policies.[9,10]

Precise measurements of isotopologues of nitrous oxide (i.e. $^{14}N^{15}N^{16}O$, $^{15}N^{14}N^{16}O$ and

$^{14}N^{14}N^{18}O$) provide a useful constraint to quantify contributions from different N_2O sources*. The major source of N_2O is microbial production in natural and agricultural soils, by both nitrifying and denitrifying bacteria. A number of studies have shown that the isotopic composition of N_2O can be used to distinguish between different microbial source pathways: The bulk ^{15}N composition of N_2O indicates the contribution of natural versus fertilized agricultural soil emissions,[7,11,12] while the site preference is independent of the reaction substrate and can be used to quantify different microbial processes, ie. nitrification versus denitrification.[11–13] Relationships between $\delta^{15}N^{\alpha}$, $\delta^{15}N^{\beta}$ and $\delta^{18}O$ indicate the relative importance of N_2O reduction to N_2, and the oxygen isotopic composition also reflects the water in the environment where N_2O was formed.[14–17] In the troposphere, N_2O is stable and the major sink is transfer to stratosphere, where N_2O is destroyed photolytically. UV photolysis is shown to produce a strong enrichment in $\delta^{18}O$ and $\delta^{15}N$ of the residual N_2O, in particular, the central position ^{15}N ($^{15}N^{\alpha}$).[18–20] This enrichment in $^{15}N^{\alpha}$ can be a particularly powerful tracer to quantify the magnitude of troposphere-stratosphere exchange, which is one of the largest uncertainties in the global N_2O budget.[21] The $\delta^{15}N$ and $\delta^{18}O$ composition of ambient N_2O shows a definite decreasing trend over the past decades, reflecting the increasing contribution of anthropogenic emissions, while observed trends in site preference remain inconclusive.[5,7,22,23]

Until recently, isotopic measurements of N_2O have used the traditional technique of flask sampling followed by laboratory-based isotope ratio-mass spectrometry (IR MS). While this technique shows excellent precision for $\delta^{18}O$ and $\delta^{15}N$, it is unsuitable for field deployment, and continuous monitoring with high time resolution is technically challenging. In addition, site preference measurements are complicated by scrambling in the ion source, non-mass-dependent oxygen isotope composition, and mass interferences such as CO_2.[24–27] Unlike IR MS, Tunable Infrared Laser Direct Absorption Spectroscopy (TILDAS) measures fundamental rovibrational bands of nitrous oxide isotopologues in the mid-infared regions at high precision, thus the technique can be used to directly distinguish between $^{15}N^{\alpha}$ and $^{15}N^{\beta}$. TILDAS techniques have been applied to a number

*Site specific ^{15}N composition: $^{14}N^{15}N^{16}O = {}^{15}N^{\alpha}$ and $^{15}N^{14}N^{16}O = {}^{15}N^{\beta}$. Site preference in ^{15}N composition: $SP = {}^{15}N^{\alpha} - {}^{15}N^{\beta}$. Bulk ^{15}N composition: $(\delta^{15}N^{\beta} + \delta^{15}N^{\beta})/2 = {}^{15}N_{bulk}$. See Toyoda et al. (2013)[5] for a detailed account of isotope notation and terminology.

of isotopic systems such as CO_2 and O_3.[28,29] Several recent studies have shown the potential of TILDAS measurement coupled to a preconcentration unit for continuous, online measurement of N_2O isotopic composition.[30–33]

This study presents a new instrument that will be used to conduct online, real-time measurements of N_2O istopic composition at Mace Head Atmospheric Research Station, Ireland, as part of the AGAGE network (http://agage.eas.gatech.edu). A cryogen-free preconcentration unit with no chemical traps was developed to allow continuous, long-term monitoring at this remote site with minimal maintainance. For the first time, isotopic reference gases labelled for both $\delta^{18}O$ and site-specific $\delta^{15}N$ isotopic compositions were synthesised and measured with both IR MS and TILDAS. A comprehensive treatment of matrix dependence for TILDAS results is presented, as well as cross-calibration of site-specific isotope ratios against IR MS method, with an investigation of scrambling corrections for IR MS. Ambient air measurements and TILDAS to IR MS comparison show that TILDAS is both accurate and precise enough to observe ambient changes in $\delta^{18}O$, $^{15}N^{\alpha}$ and $^{15}N^{\beta}$ of N_2O with a temporal resolution of 0.5-2 hours.

2 Materials and methods

2.1 Fully-automated cryogen-free N_2O preconcentration

For N_2O preconcentration, we use a modified Medusa system[34] known as 'Stheno II'[†]. Medusa is a fully-automated cryogen-free preconcentration unit coupled to GC/MS used to measure a number of CFCs and other non-CO_2 greenhouse gases at AGAGE stations;[34] a similar system has been used previously to preconcentrate N_2O for isotope measurements.[32,35] The preconcentration procedure involves collecting N_2O on a glass beads trap at approximately -156°C and is described in detail in Section S1 of the supplementary material. Our system differs from previous preconcentration units used for spectroscopic measurements[31–33] in a number of ways, most notably, it uses

[†]The 'Stheno II' unit discussed here is a new unit, improving upon the principles used for the original 'Stheno' preconcentration unit described in Potter et al. (2013)[35]

a glass beads trap rather than a HayeSep D trap to adsorb N_2O, and CO_2 is not removed from the sample air stream. These changes allow long-term operation with minimal maintenance. A basic schematic of the preconcentration unit is shown in Figure 1 and an example of the preconcentration/trapping routine is presented in Figure 2.

2.2 Spectroscopic analysis of N_2O isotopic composition with TILDAS

Spectroscopic measurements are made with a dual-laser TILDAS instrument (Aerodyne Research Inc), shown as the 'laser cell' in Figure 1. The instrument has two lasers tuned to 2188 and 2203 cm^{-1} to measure the four isotopocules of N_2O, as shown in Figure 3. The spectroscopic measurements are described in detail in Section S2 of the supplementary material. Measurements are made at a pressure of 10 mbar with an N_2O mixing ratio of 65 ppm and a CO_2 mixing ratio of 8% (see Section S2.4). Standards are run between every sample peak, as shown in Figure 2 (standards are discussed in Section S2.2). Following acquisition of the raw concentration data, corrections are made to account for background, matrix effects, and calibration to the international isotopic standard scale. The data analysis procedure and associated corrections are described in detail in Section S2 of the supplementary material, and an example of the data analysis cycle is shown in Figure S2.

2.3 Synthesis of standards by NH_4NO_3 decomposition

A range of isotopic standards were synthesised via NH_4NO_3 decomposition to compare isotopic measurements between IR MS and TILDAS. The synthesis is described in detail in Section S3 of the supplementary material and only a brief description will be given here. NH_4NO_3 with a range of isotopic compositions was produced from recrystallizing stock NH_4NO_3 with isotopic spikes of $Na^{15}NO_3$, $Na^{14}NO_3$, $^{15}NH_4Cl$ and $^{14}NH_4Cl$, as well as equilibration with $H_2\,^{18}O$. The NH_4NO_3 was flame-sealed into glass tubes and decomposed at 270°C to form N_2O, which was purified by distillation with dry ice-ethanol and liquid nitrogen.[36] Five standards were produced with varying ^{15}N and ^{18}O compositions, as detailed in Table S2.

2.4 Analysis of N_2O isotopic composition with isotope ratio-mass spectrometry

Isotopic composition of N_2O standard gases was measured with IR MS (Thermo Electron MAT 253). Pure N_2O was used for analyses; gas chromatographic analysis with a thermal conductivity detector (TCD) showed no detectable CO_2 in N_2O samples derived from NH_4NO_3 decomposition (see Figure S6). Following Toyoda and Yoshida (1999), N_2O^+ (masses 44, 45 and 46) and NO^+ (masses 30 and 31) ions were measured to determine position-specific ^{15}N substitutions.[25,27] Analysis conditions are summarised in Table S3, and NO^+ ion scrambling factors are discussed in Section 3.1.2.

3 Results and discussion

3.1 Comparison of TILDAS and IR MS measurements

The five N_2O standards synthesised by ammonium nitrate decomposition (Table S2) as well as the two laboratory reference gases Ref I and Ref II were measured with IR MS and TILDAS in order to cross-calibrate the TILDAS and IR MS measured isotopologue ratios and investigate the accuracy of the two techniques considering IR MS scrambling factors and TILDAS matrix corrections. The results are presented in Table S4 and summarised in Figure 4, and show very good agreement between the IR MS and TILDAS for most samples. The instrument comparison shows that TILDAS is able to provide accurate results across a wide range of N_2O, CO_2 and bath gas compositions and N_2O isotopic compositions. TILDAS measurements at 23.5 and 40.5 ppm N_2O are not accurate: at $[N_2O] <$ approximately 45 ppm (at 0.010 atm, 1.7×10^{13} molec cm^{-3}) peaks are too small for fitting ($<$4% absorption depth) and results are not accurate. Sufficient N_2O should be trapped to achieve at least 45 ppm in the cell at 0.010 atm, corresponding to $\sim$1 L of air at a typical atmospheric N_2O mixing ratio of 327 ppb.

3.1.1 Matrix effects on spectroscopic line shape and measurement accuracy

The composition and pressure of the matrix has a significant effect on line shape, and thus on data fits and measurement accuracy. Samples (trapped ambient and compressed air) and standards are therefore matrix-matched as closely as possible. Measurement accuracy was tested across a range of matrix compositions. A brief description of the results is given here; full details are presented in Section S2.4 of the supplementary material. The primary matrix gas in the laser cell is zero air, hereafter referred to as the 'bath gas'; the N_2:O_2 ratio of the bath gas does not have any significant effect on the peak shape (Figure S4) or on measurement accuracy, as shown with measurements of Ref II in a bath gas of 100% N_2 and 100% O_2 (Figure 4). The total pressure of bath gas, on the other hand, has a significant effect on the results, affecting measured isotopic composition by $\sim$2.6-6‰ mbar^{-1}. The measurement pressure for standards is therefore regulated by the bulk expansion volume pressure ($\sim$750 mbar; Section S2.2) in the 'standard reservoirs' shown in Figure 1, while the pressure for trapped sample measurements is controlled to within $\pm$2% by the length of the flush into the cell ($\sim$90 seconds; Section S1 and Figure 2). An empirical pressure correction is applied to account for the small differences in pressure that remain ($\pm$0.3 mbar; Section S2.3).

The CO_2 partial pressure affects the measurement accuracy with the same order of magnitude as the bath gas pressure ($\sim$2.6-4‰ mbar^{-1}; Table S1 and Figure S3), however it cannot be controlled in trapped samples as the ambient pressure of CO_2 shows significant temporal variation, for example $>$10% at Mace Head Station.[37,38] A pressure correction is therefore also applied to account for differences in CO_2 partial pressure, in addition to the pressure correction for bath gas pressure (Section S2.3). The empirically-determined pressure dependencies are highly linear over the range of interest and show less than 5% change over longer time periods (Section S2.4, Table S1); therefore they introduce <0.05‰ error under normal measurement conditions. Ref II was measured in a matrix with 14% CO_2 equivalent to an ambient mixing ratio of 700 ppm, requiring pressure corrections of -1.73$\pm$0.09‰, 1.67$\pm$0.08‰ and -2.56$\pm$0.13‰ for $\delta^{15}N^{\alpha}$, $\delta^{15}N^{\beta}$ and $\delta^{18}O$ respectively. The pressure-corrected measurement showed very good agreement with IR MS and other TILDAS results, as shown in Figure 4 and Table S4.

The pressure dependence of isotopic measurements is most likely caused by changes in peak shape and broadening in response to different matrix gases. Peak width in the TDL Wintel software used for spectroscopic data analysis (Aerodyne Research, Inc.) is described by an approximated Voigt profile, which can be deconvolved into contributions from the gaussian Doppler line shape function and the Lorentz line shape function due to pressure broadening.[39] Both Gaussian and Lorentzian line widths were estimated as a function of pressure (see Figure S7) by fitting measured spectra to a Voigt profile to find an optimum fit and exact width. The extent of pressure broadening and Dicke narrowing were estimated for comparison with literature values from the HITRAN database.[40,41] The measurements and calculations are presented in Section S4 of the supplementary material; the results will be described here. [‡]

The parameters describing peak shape are summarised in Table 1. For all four N_2O peaks, it can be seen that the derived air broadening coefficients are consistently higher than given in the HITRAN database: $\sim$2% for $^{14}N^{14}N^{16}O$ and $^{14}N^{14}N^{16}O$ (within the uncertainty of HITRAN data), 6% for $^{15}N^{14}N^{16}O$ and 8% for $^{14}N^{14}N^{18}O$ (significantly different to HITRAN data[42–44]). The HITRAN values for N_2O are measured at high pressures ($>$0.09 atm,[42,43]) relative to the pressures at which these measurements were made ($\sim$0.01 atm); more importantly, while the HITRAN line widths and strengths are taken from measurements of both $^{14}N^{14}N^{16}O$ and the minor isotopes, the HITRAN broadening coefficients are taken from measurements of only $^{14}N^{14}N^{16}O$.[42–44]

Although the estimate of Dicke-narrowing factor[45] (Eq. S7) is based only on a parameterisation and the effects of narrowing are expected to be largest at $\sim$0.06-0.07 atm,[46] the results clearly show that there is significant narrowing at the low pressures used in the TILDAS cell. At measurement pressure of 10 mbar (0.01 atm), the Doppler width (2-2.3 cm^{-1} for the four N_2O peaks; see Figure S7) contributes a large part of the total Voigt line width (2.4-2.8 cm^{-1}). Dicke narrowing has a significant impact on the Doppler width and the fit, accounting for $\sim$50% of peak width change with pressure, and thus it is an important feature needed to gain accurate and precise results. We have implemented this narrowing into our fits and find a significant improvment in precision of

[‡]Pressure is in units of atmospheres (atm) in this section for consistency with the HITRAN database.

repeated measurements on the order of 3-4×; eg. precision on $\delta^{15}N^{\alpha}$ is 0.25-0.4‰ without the 'Dicke factor' and improves to 0.07-0.15‰ when the 'Dicke factor' is included in the fit.

3.1.2 Scrambling in the ion source in IR MS analyses

Site-specific N_2O isotopic composition is measured indirectly in the IR MS, by monitoring the isotopic composition of N_2O^+ ions (*m/z* = 44, 45, 46) and NO^+ ions (*m/z* = 30, 31). $^{15}NO^+$ ions result primarily from fragmentation of $^{14}N^{15}NO$, thus the site-specific isotopic composition can be inferred.[24–26] This method is complicated by scrambling in the ion source, which means that ∼8% of $^{15}NO^+$ is actually derived from $^{15}N^{14}NO$, and also replies on the assumption that the oxygen isotopic composition is mass-dependent.[27] This assumption is the reason why the site-specific isotopic composition for 448-H sample, which is strongly enriched in ^{18}O, is poorly characterised with IR MS measurements, as shown in Figure 4: the directly-measured value of $\delta^{18}O$ (mass 46) is used to infer $\delta^{17}O$ according to a mass-dependent relationship (Eq. 9 in the supplementary material). The inferred $\delta^{17}O$ is then used to iteratively calculate site-specific ^{15}N isotopic composition from masses 45 ($^{15}N^{14}N^{16}O^+$, $^{14}N^{15}N^{16}O^+$ and $^{14}N^{14}N^{17}O^+$) and 31 ($^{15}N^{16}O^+$ and $^{14}N^{17}O^+$) (see Eqs. 10, 11 and 13 in the supplementary material). Thus, if the sample oxygen isotopic composition is not mass-dependent, the calculated values of $\delta^{17}O$ and thus site-specific N_2O isotopic composition are incorrect. In contrast, TILDAS is able to accurately measure site-specific ^{15}N substitutions across a large range of $\delta^{17}O$, $\delta^{18}O$ and $\Delta^{17}O$ values.

Scrambling in the ion source was considered by comparing the measured isotopic composition of the standards (not including 448-H), which have site preference values ranging from -1.76 to +15.09‰, between the IR MS and the TILDAS. Although the TILDAS values have an associated measurement error, the site-specific ^{15}N substitutions are directly measured, thus there is no systematic relationship between site preference and error. Averaging across all the seven standards can therefore give an accurate view of IR MS measurement quality without a bias from TILDAS measurement uncertainty. The calculations used for the scrambling corrections (from[25,27,47]) are presented in Section S5 of the supplementary information and the results are summarised in Figure

5. Two possible scrambling models are considered:

- 'one factor' scrambling, with equal yield of $^{15}NO^+$ from $^{15}N^{14}NO$ and $^{14}NO^+$ from $^{14}N^{15}NO$ described by a single scrambling factor 'γ', ie. γ of 0.08 means 8% of $^{15}NO^+$ is derived from $^{15}N^{14}NO$ and similarly for $^{14}NO^+$

- 'two factor' scrambling, where the scrambling of $^{14}N^{15}NO$ (γ^α) is not equal to the scrambling of $^{15}N^{14}NO$ (γ^β) (differences due to other isotopic substitution possibilities are not accounted for, eg. clumped, ^{17}O, ^{18}O)

More complex scrambling models have also been considered[27] however the number of standards in this study is too small to consider the accuracy of models with a larger number of variables.

In agreement with the results of Westley et al.,[27] scrambling is more complex than a one-factor scrambling model can account for: The IR MS and TILDAS results never agree within the measurement error (Figure S8) with the one factor correction. Overall, best agreement is seen for one factor scrambling with γ = 8%, consistent with results obtained using similar source conditions.[24,25,27] However, for calculation of $\delta^{15}N^\alpha$, best agreement is obtained with a scrambling factor of 9%, highlighting the limitations of the one-factor model.

The results from comparison of IR MS and TILDAS with two-factor scrambling show $\sim$0.05‰ improvement in accuracy for the IR MS measurement compared to one-factor scrambling. The accuracy of results is much more sensitive to the scrambling of $^{14}N^{15}NO$ (γ_α) than $^{15}N^{14}NO$ (γ_β). From consideration of $\delta^{15}N^\alpha$, $\delta^{15}N^\beta$ and site preference, it is clear that the optimal value of γ_α is 8-9%, in agreement with previous studies,[24,25,27] while the optimal value of γ_β is clearly lower - between 2 and 4%. This value is much lower than reported by previous studies (eg. single factor of 8.5% from Brenninkmeijer et al. 2009;[24] γ_β of $\sim$9% from Westley et al. 2007[27]). This study presents the widest range of isotopic references gases yet considered and does not rely on primary calibration through techniques such as NH_4NO_3 decomposition or enriched gas mixing,[24,25,27,47] which give uncertainties of >0.2-0.3‰ in site preference, but instead presents the first laser spectroscopy-calibrated consideration of IR-MS scrambling. The accuracy of standard

site preference values in previous studies may not have been high enough to fully assess the optimum value of γ_β, considering that the calculated site preference is much less sensitive to the chosen value of γ_β than the value of γ_α.

Even with the optimised two-factor scrambling model, correcting for scrambling in the ion source introduces an error larger than the combined IR MS and TILDAS measurement uncertainty for both $\delta^{15}N^{\alpha}$ and site preference ($\delta^{15}N^{\beta}$ is accurate to within the measurement uncertainty). The error that is introduced depends on the site preference value of the N_2O being considered, therefore both measurement precision and accuracy are affected. This limits the potential of IR MS measurements for high-precision monitoring of site-specific N_2O isotope ratios in lab and field studies, particularly at remote background sites like Mace Head where relevant changes in isotopic composition are very small.

3.2 Isotopic measurements in preconcentrated samples

3.2.1 Trapping efficiency: Trace gas recovery

Quantitative recovery of N_2O following trapping is critically important to prevent introduction of isotope fractionation by absorption/desorption processes.[48,49] Unlike previous instruments,[31–33] the Stheno II preconcentration unit (and the predecessor Stheno I[35]) uses a glass beads trap instead of the stronger HayeSep D adsorbent. The major advantage of the glass beads trap is that no N_2/O_2 is trapped from the air; thus, the bath gas is added as a flush with a known composition, making the pressure and matrix easier to accurately control. The range over which glass beads can efficiently trap N_2O was investigated by trapping increasing amounts of sample and comparing the measured and expected N_2O and CO_2 concentrations, as shown in Figure 6. N_2O is efficiently trapped when the sample volume is $<$4 L; CO_2 is efficiently trapped until $\sim$2 L. It is desirable to use the minimum trapped volume, to conserve sample when measuring flask samples and to achieve the highest possible time resolution when making continous ambient measurements, however at N_2O mixing ratios $<$45 ppm (at 10 mbar total cell pressure) isotopic analysis is no longer accurate (see Section 3.1). The 'optimal trapping range' is therefore 1200-1800 mL of ambient air. Within this

range, N_2O recovery is >99% and therefore the fractionation introduced by trapping is negligible.

3.2.2 Measurements of N_2O isotopic composition in ambient samples from Cambridge, Massachusetts

N_2O isotopic composition was measured continuously from MIT's 'Green Building' for two weeks between March 3-16, 2013. The sampling inlet was located on the roof of the 18-story (95 m) building and connected to sampling pumps (see Figure 1) with >50 m of Synflex 1300 tubing (Eaton Corporation, USA). Samples were measured every 28 minutes, and for every 5-10 ambient air samples, one compressed air sample (Medical grade, Airgas Inc.) was measured to monitor trapping efficiency and precision. The compressed air measurements and precision histograms are shown in Figure S9; the capabilities of the instrument are summarised in Table 2. Precision is better for $\delta^{15}N$ than $\delta^{18}O$ due to the relatively small absorption depth of the $^{14}N^{14}N^{18}O$ peak (Figure 3).

Ambient air measurements over the 13-day period are shown in Figure 7. The scatter in ambient air measurements ('true' variability + measurement error; bars in Figure 7 histograms) was compared to the scatter in compressed air measurements (measurement error only; smooth line in Figure 7 histograms), to determine if the instrument precision is sufficient to see changes in isotopic composition of ambient air. $\delta^{18}O$ values show a large amount of true variability over the measurement period, thus although precision is lowest for this isotopocule, the precision is sufficient to observe ambient variations for both single measurement and four-point moving average. For $\delta^{15}N^{\beta}$, there is some true variability outside the measurement error with single measurements, although the difference between frequency distributions is much clearer for the four-point average data. The true variability is smaller than the measurement error of single measurements for both $\delta^{15}N^{\alpha}$ and $\delta^{15}N_{bulk}$; true variability of these isotopocules can only be resolved using the four-point moving average.

The isotopic measurements were compared to weather variables to examine causes of variability in isotopic composition. The weather data is shown in Figure S10 and correlations are

summarised in Table S5 in the supplementary material. All four isotopomers show a significant relationship to pressure; a positive correlation for $\delta^{18}O$ and a negative correlation for all ^{15}N isotopomers. This correlation may relate to exchange of free tropospheric air. Relative humidity showed a significant correlation with all isotopocules except $\delta^{15}N^{\alpha}$. It is possible that this relates to partitioning between different microbial pathways. Wind direction showed a significant relationship to $\delta^{15}N^{\beta}$, with slightly isotopically heavier N_2O originating from the continent and isotopically light N_2O from the marine sector. A full investigation of the relationship between meteorological variables and measured isotopic composition is beyond the scope of this study and will be discussed in a later publication.

4 Conclusions

Measurement of N_2O isotopic composition has traditionally involved the collection of flask samples, which are then purified and measured with IR MS in a laboratory. While this technique has yielded interesting results, potential for investigations of seasonal cycles or changes in sources related to meteorology is limited by the feasible number and temporal resolution of samples. Using preconcentration without CO_2 removal followed by TILDAS, we have obtained sufficient precision with a four-point moving average of 28-minute measurements to observe ambient remote-site changes in all the isotopocules of N_2O, and we have demonstrated accuracy across a wide range of isotopic composition and site preference values. The 'Stheno II' instrument is automated and remotely operated, and uses very few consumables, to be well-suited for remote deployment at sites such as Mace Head Atmospheric Research Station.

The time series in Figure 7 shows that there is significant variability in N_2O isotopic composition on very short time scales. The data shows decoupling between ^{15}N and ^{18}O content of N_2O. Variability in $\delta^{18}O$ is larger than variability in $\delta^{15}N^{\beta}$, which is in turn greater than variability in $\delta^{15}N^{\alpha}$ and $\delta^{15}N$ bulk. The isotopic composition of N_2O reflects sources, sinks and transport, and the rich data set that can be obtained from 'Stheno II' provides constraints on these processes. In

combination with inverse modelling and analysis of other trace gases and meteorological variables, the results can be used to provide new insight into N_2O variability.

Acknowledgments

We thank S. Toyoda and N. Yoshida at Tokyo Tech for calibration of reference N_2O, and S. O'Doherty, D. Young and G. Spain for helpful suggestions regarding field deployment. We acknowledge NSF Grant #0959280 "MRI-R2: Development and Deployment of Automated Continuous Wave Quantum Cascade Laser Instruments for On-Site Monitoring of the Four Isotpomers of Nitrous Oxide" for supporting this work.

Figures and Tables

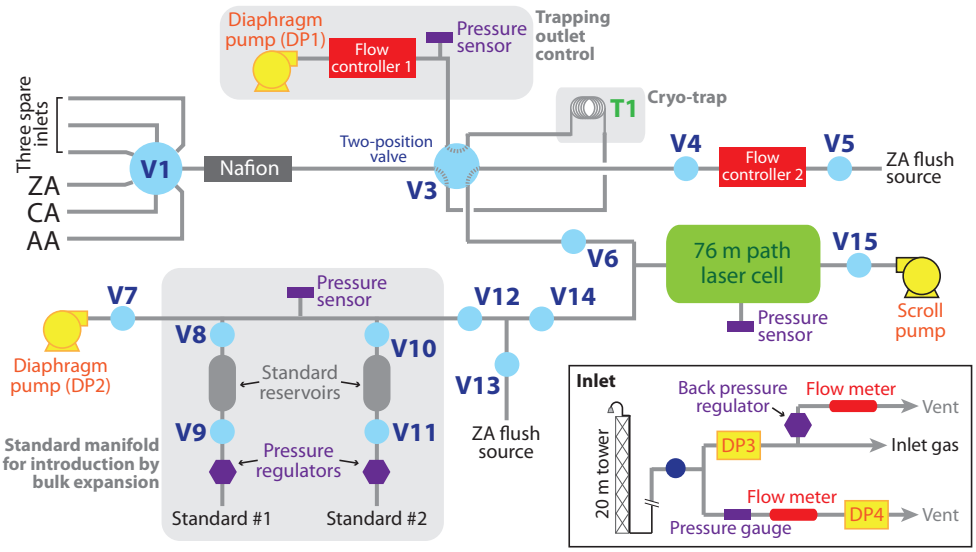

Figure 1: Schematic of the modified Medusa system 'Stheno II', developed for preconcentration of N_2O without the use of chemical traps or liquid nitrogen. 'V' specifies a valve, 'T' is a trap, 'DP' specifies a diaphragm pump, 'ZA' = zero air, 'AA' = ambient air, 'CA' = compressed air. The instrument is shown with valve #3 in the 'trapping' position. The system is described in detail in Section S1 of the supplementary material.

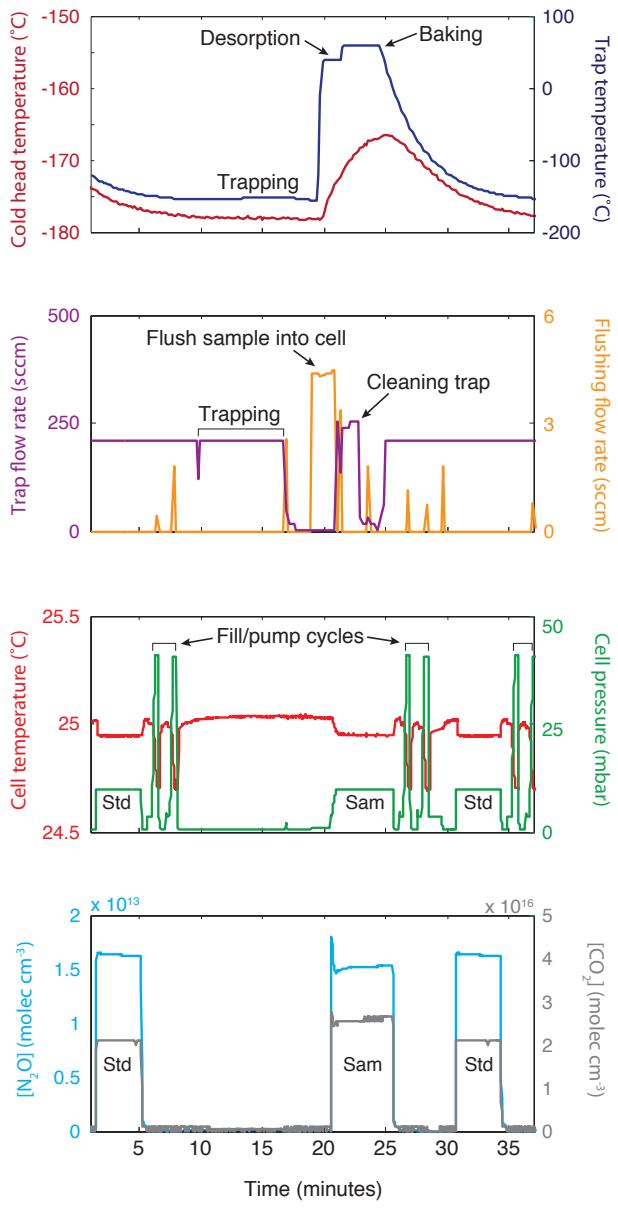

Figure 2: Trapping routine used for N_2O preconcentration on a liquid-nitrogen free glass beads trap, coupled to TILDAS isotope measurement. The first panel shows the cold head (red) and trap (blue) temperatures. The second panel shows the flow rate through the trap (purple; both flush and sample) and the flushing flow used to push the sample into the laser cell (orange; spikes are due to multiport valve switching and do not affect measurement). The third panel shows the pressure (green) and temperature (red) in the laser measurement; the periods where the cell is cleaned are indicated, and 'Std' refers to a standard while 'Sam' refers to a sample. The fourth panel shows the concentration (molec cm^{-3}) of N_2O (major isotope; blue) and CO_2 (grey) measured in the laser cell.

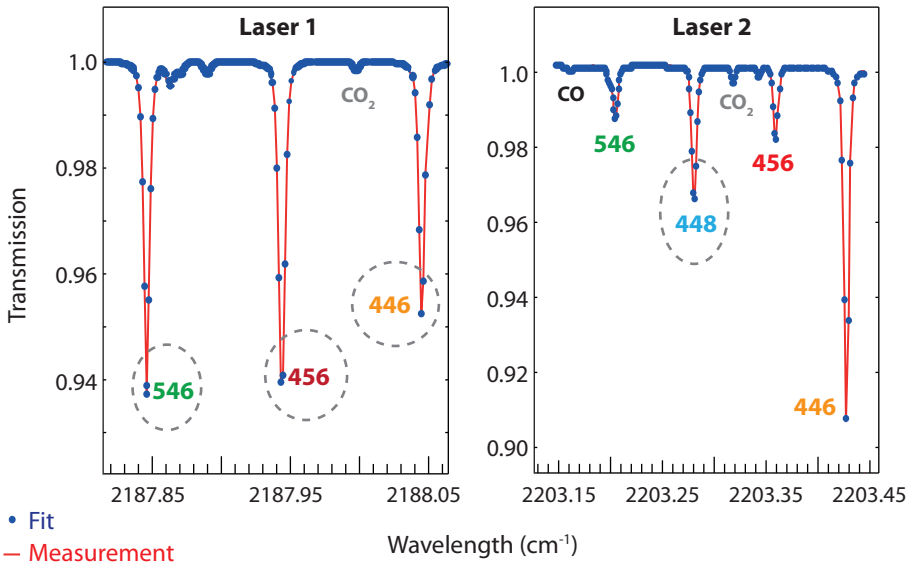

Figure 3: Measured (blue dots) and fitted (red line) spectra for Laser 1 (2188 cm^{-1}) and Laser 2 (2203 cm^{-1}). The peaks used for isotope measurements are circled with a gray dashed line. Measurement conditions: 8.9% CO_2, 69.5 ppm N_2O in synthetic air, P = 11.9 mbar, T = 298 K, path = 76 m. The HITRAN lines and simulated ($\equiv$ expected) spectra for the two lasers are shown in Figure S1 for comparison with the measured and fitted spectra.

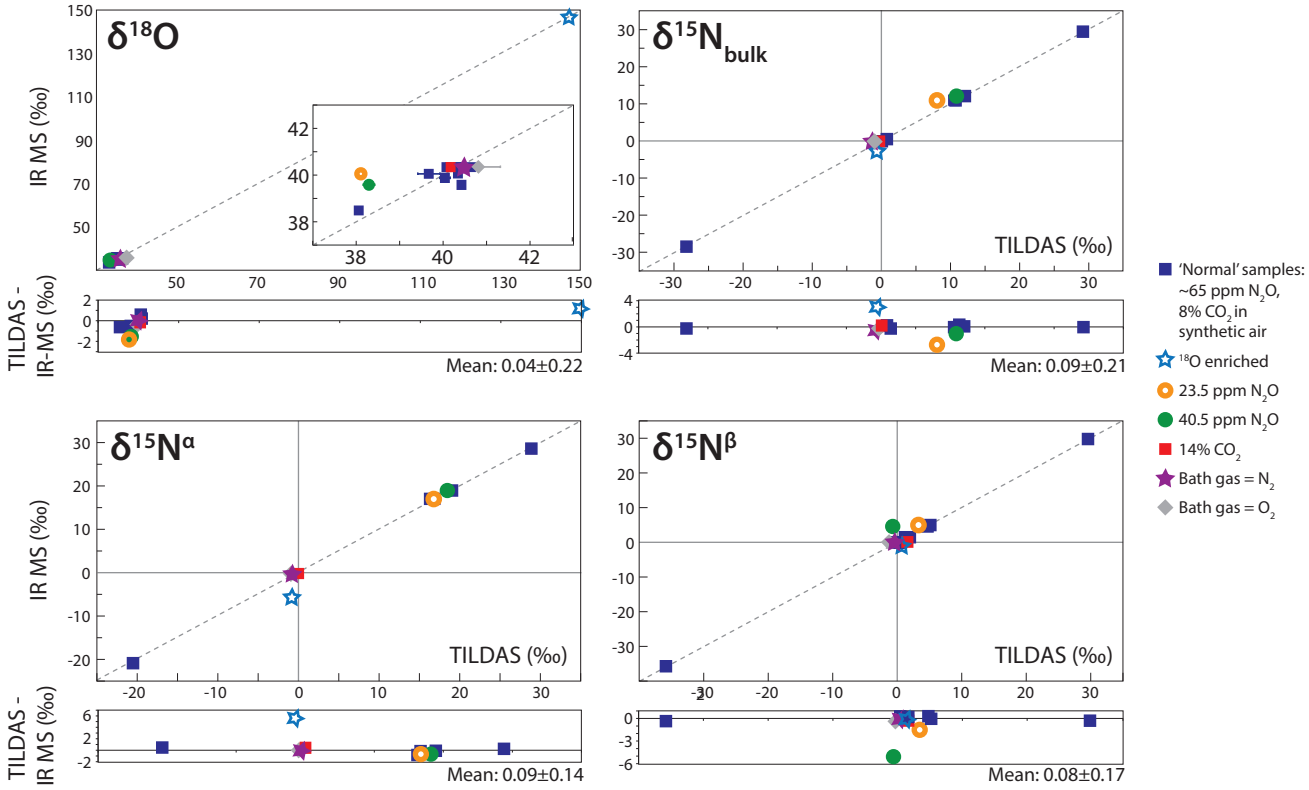

Figure 4: Comparison of N_2O isotope ratios measured with IR MS (y-axis) and TILDAS (x-axis) for the four isotopocules of N_2O. The offsets between the two techniques (TILDAS - IR MS) are shown under each plot. The exact values can be seen in supplementary Table S4. The majority of samples were measured in the normal matrix (blue squares) but accuracy was tested across several matrix pertubations: low N_2O mixing ratio (yellow open and green filled circles), high CO_2 mixing ratio (red squares), and N_2 and O_2 bath gases (purple star and grey diamonds respectively). ^{18}O enriched samples are indicated with open blue stars due to importance of ^{18}O composition when calculating site-specific ^{15}N composition of N_2O with IR MS.

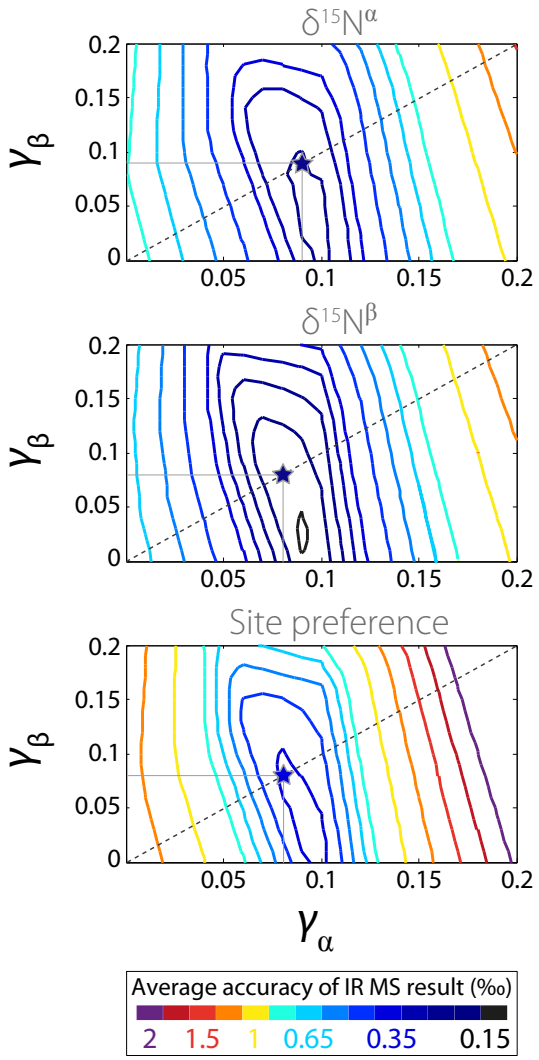

Figure 5: Absolute accuracy of site-specific N_2O isotopic measurements made with IR MS (defined as $\mid (\delta^{15}N^{\alpha})_{\text{IRMS}} - (\delta^{15}N^{\alpha})_{\text{TILDAS}} \mid$ averaged across the six N_2O standards, and similarly for $\delta^{15}N^{\beta}$ and site preference). Two-factor scrambling results are shown with the contour plot: γ^{α} (x-axis) shows the scrambling of $^{14}N^{15}NO$, and γ^{β} (y-axis) shows the scrambling of $^{15}N^{14}NO$. The lowest point of the contour plot shows the optimum scrambling factors. The dashed line indicates where both factors are equal, which is equivalent to the one-factor scrambling model. The star indicates where the deviation for the one factor model is at a minimum (see Figure S8 for a full plot of one-factor scrambling results).

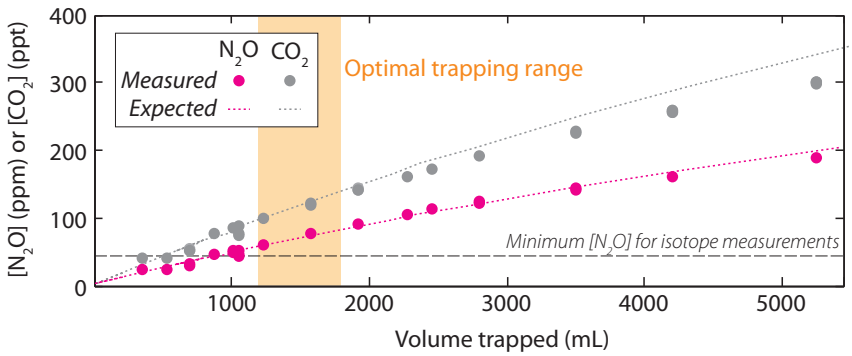

Figure 6: Measured (circles) and expected (dotted lines) mixing ratios of N_2O and CO_2 as the volume of air trapped is increased from 400 to 5200 mL. The expected mixing ratio is curved with respect to volume trapped as the cell pressure also increases when a greater quantity of gas is trapped. The dashed line shows the minimum N_2O mixing ratio (at 10 mbar total cell pressure) required for accurate isotope analysis. Testing was performed with a flow rate of 370 sccm; further tests showed trapping efficiency is not affected by trapping flow rate up to 500 sccm.

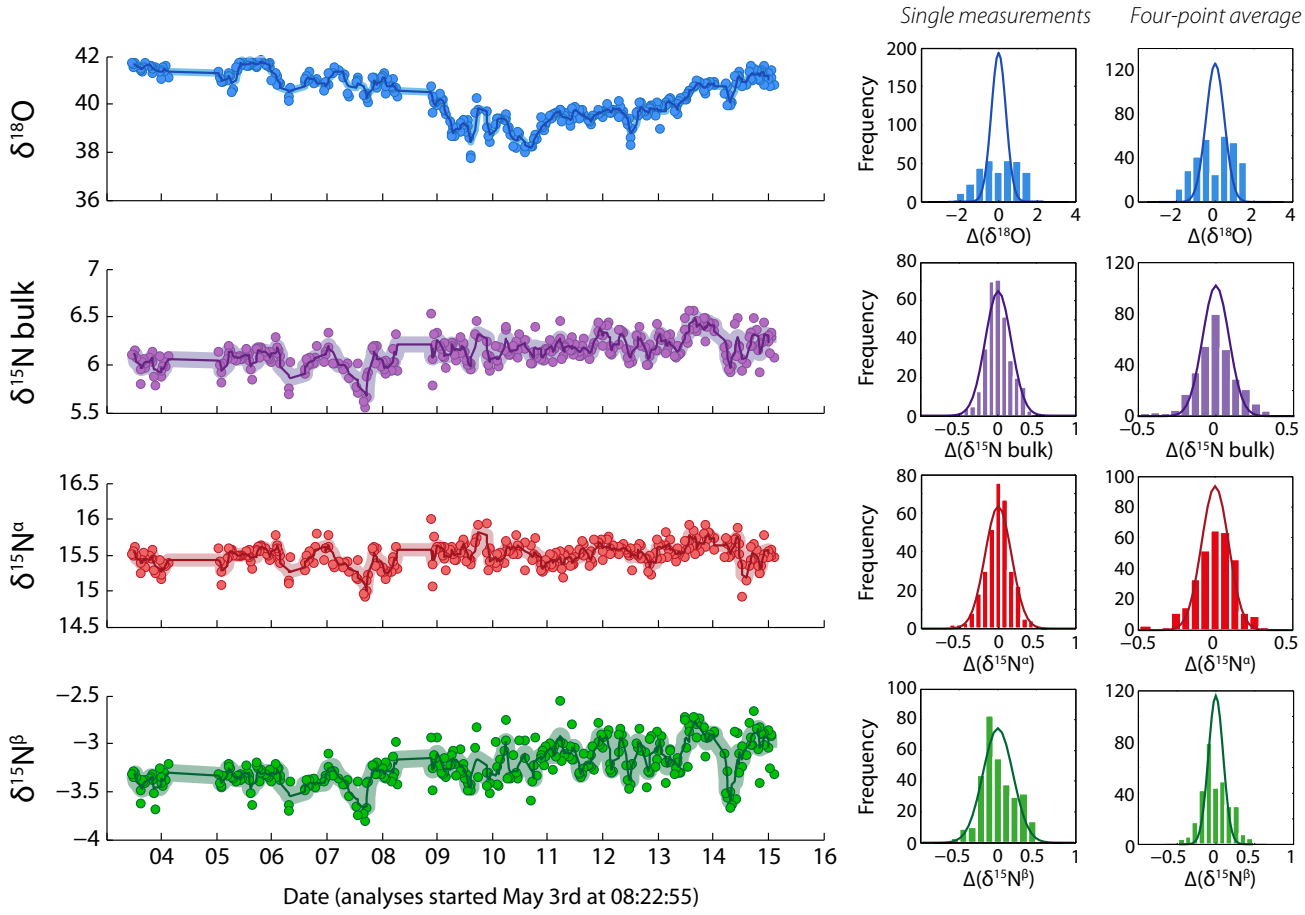

Figure 7: N_2O isotope ratios from repeated measurements of ambient air in Cambridge, MA. Left-hand panels show measured isotopic composition with time: points are individual measurements, and thick lines show the 4-point moving average. The thickness of the line corresponds to the 1σ error determined from repeated measurements of compressed air: 0.16, 0.08, 0.085 and 0.095‰ for $\delta^{18}O$, $\delta^{15}N_{bulk}$, $\delta^{15}N^{\alpha}$ and $\delta^{15}N^{\beta}$ respectively. Right-hand panels show the frequency distribution of deviations from the mean value in permil for single measurements and for four-point moving averages; ie. $\Delta(\delta^{18}O) = \delta^{18}O_x$ - mean($\delta^{18}O$). Bars show the measured frequency distribution for ambient air measurements, while lines show the expected Gaussian distribution based on random error only, determined from repeated measurements of compressed air.

Table 1: Air-, self- and CO_2-broadening coefficients in cm^{-1} atm^{-1} for N_2O and CO_2 peaks measured by varying air (bath gas) pressure between 0.0076 and 0.0113 atm and CO_2 pressure between 0.0005 and 0.0013 atm (see Figure S7). N_2O pressure was 5×10^{-7} atm, thus self-broadening of N_2O was negligible during measurements. Molecule: numbers in brackets refer to the HITRAN identification number of the molecule. Peak positions are cm^{-1}.

Molecule	**Peak position**	**Lorentz width**				**Doppler width**	
		γ_{air}		γ_{self}	γ_{CO2}	β_{air}	β_{CO2}
		HITRAN	*This study*	*HITRAN*	*This study*		
$^{14}N^{14}N^{16}O$ (41)	2188.0448	0.0838	0.0858	0.110	0.0268	3.70	9.73
$^{14}N^{15}N^{16}O$ (42)	2187.9432	0.0798	0.0812	0.104	0.0409	4.05	16.56
$^{15}N^{14}N^{16}O$ (43)	2187.8460	0.0774	0.0837	0.101	0.0408	5.53	14.97
$^{14}N^{14}N^{18}O$ (44)	2203.2808	0.0774	0.0818	0.101	0.0286	4.84	11.91

Table 2: Summary of the precision attainable with TILDAS measurements of N_2O isotopic composition. 'Precision' is the 1σ standard deviation of repeated measurements of compressed air. $n_{averaged}$ is the amount of measurements that need to be averaged to achieve a certain precision.

	$\delta^{18}O$	$\delta^{15}N^{\alpha}$	$\delta^{15}N^{\beta}$	$\delta^{15}N_{bulk}$
Precision (‰), 28 min time resolution	0.32	0.17	0.19	0.16
$n_{averaged}$ for <0.2‰ precision	3	No averaging required		
Temporal resolution (hours)	1.4	0.5	0.5	0.5
$n_{averaged}$ for <0.1‰ precision	11	3	4	3
Temporal resolution (hours)	5.1	1.4	1.9	1.4

References

(1) IPCC, In *Contribution of Working Group I to the Fourth Assessment Report of the Intergovernmental Panel on Climate Change*; Solomon, S., Qin, D., Manning, M., Chen, Z., Marquis, M., Averyt, K. B., Tignor, M., Miller, H. L., Eds.; Cambridge University Press, 2007.

(2) Ravishankara, A. R.; Daniel, J. S.; Portmann, R. W. *Science* **2009**, *326*, 123–125.

(3) Khalil, M. a. K.; Rasmussen, R. a.; Shearer, M. J. *Chemosphere* **2002**, *47*, 807–21.

(4) Park, S.; Croteau, P.; Boering, K. A.; Etheridge, D. M.; Ferretti, D.; Fraser, P. J.; Kim, K. . R.; Krummel, P. B.; Langenfelds, R. L.; van Ommen, T. D.; Steele, L. P.; Trudinger, C. M. *Nature Geoscience* **2012**, *5*, 261–265.

(5) Toyoda, S.; Kuroki, N.; Yoshida, N.; Ishijima, K.; Tohjima, Y.; Machida, T. *Journal of Geophysical Research - Atmospheres* **2013**, *118*, 1–13.

(6) Sowers, T.; Rodebaugh, A.; Yoshida, N.; Toyoda, S. *Global Biogeochem. Cycles* **2002**, *16*, 1129.

(7) Rockmann, T.; Kaiser, J.; Brenninkmeijer, C. A. M. *Atmospheric Chemistry and Physics* **2003**, *3*, 315–323.

(8) Wolf, B.; Zheng, X.; Brüggemann, N.; Chen, W.; Dannenmann, M.; Han, X.; Sutton, M. a.; Wu, H.; Yao, Z.; Butterbach-Bahl, K. *Nature* **2010**, *464*, 881–4.

(9) Nishina, K.; Akiyama, H.; Nishimura, S.; Sudo, S.; Yagi, K. *J. Geophys. Res.* **2012**, *117*, G04008–.

(10) Cavigelli, M. A.; Grosso, S. J. D.; Liebig, M. A.; Snyder, C. S.; Fixen, P. E.; Venterea, R. T.; Leytem, A. B.; McLain, J. E.; Watts, D. B. *Frontiers in Ecology and the Environment* **2012**, *10*, 537–546.

(11) Park, S.; Perez, T.; Boering, K. A.; Trumbore, S. E.; Gil, J.; Marquina, S.; Tyler, S. C. *Global Biogeochemical Cycles* **2011**, *25*, GB1001.

(12) Perez, T.; Trumbore, S. E.; Tyler, S. C.; Matson, P. A.; Ortiz-Monasterio, I.; Rahn, T.; Griffith, D. W. T. *Journal of Geophysical Research - Atmospheres* **2001**, *106*, 9869–9878.

(13) Sutka, R. L.; Ostrom, N. E.; Ostrom, P. H.; Breznak, J. A.; Gandhi, H.; Pitt, A. J.; Li, F. *Applied and Environmental Microbiology* **2006**, *72*, 638–644.

(14) Yoshinari, T.; Wahlen, M. *Nature* **1985**, *317*, 349–350.

(15) Wahlen, M.; Yoshinari, T. *Nature* **1985**, *313*, 780–782.

(16) Ostrom, N. E.; Pitt, A.; Sutka, R.; Ostrom, P. H.; Grandy, A. S.; Huizinga, K. M.; Robertson, G. P. *Journal of Geophysical Research-biogeosciences* **2007**, *112*, G02005.

(17) Snider, D. M.; Venkiteswaran, J. J.; Schiff, S. L.; Spoelstra, J. *GLOBAL CHANGE BIOLOGY* **2012**, *18*, 356–370.

(18) Rahn, T.; Zhang, H.; Wahlen, M.; Blake, G. A. *Geophysical Research Letters* **1998**, *25*, 4489–4492.

(19) Rockmann, T.; Kaiser, J.; Brenninkmeijer, C. A. M.; Crowley, J. N.; Borchers, R.; Brand, W. A.; Crutzen, P. J. *Journal of Geophysical Research* **2001**, *106*, 10403–10410.

(20) Kaiser, J.; Engel, A.; Borchers, R.; Rockmann, T. *Atmospheric Chemistry and Physics* **2006**, *6*, 3535–3556.

(21) Park, S. Y.; Atlas, E. L.; Boering, K. A. *Journal of Geophysical Research - Atmospheres* **2004**, *109*.

(22) Rahn, T.; Wahlen, M. *Global Biogeochem. Cycles* **2000**, *14*, 537–543.

(23) Röckmann, T.; Levin, I. *Journal of Geophysical Research - Atmospheres* **2005**, *110*.

(24) Brenninkmeijer, C. A. M.; Röckmann, T. *Rapid Communications in Mass Spectrometry* **1999**, *13*, 2028–2033.

(25) Toyoda, S.; Yoshida, N. *Analytical Chemistry* **1999**, *71*, 4711–4718.

(26) Kaiser, J.; Röckmann, T.; Brenninkmeijer, C. A. M. *Journal of Geophysical Research* **2003**, *108*, 4476.

(27) Westley, M.; Popp, B. N.; Rust, T. M. *Rapid Communications in Mass Spectrometry* **2007**, *21*, 391–405.

(28) Weidmann, D.; Wysocki, G.; Oppenheimer, C.; Tittel, F. K. *Applied Physics B-lasers and Optics* **2005**, *80*, 255–260.

(29) Janssen, C.; Tuzson, B. *Applied Physics B-lasers and Optics* **2006**, *82*, 487–494.

(30) Uehara, K.; Yamamoto, K.; Kikugawa, T.; Yoshida, N. *Spectrochimica Acta Part A: Molecular and Biomolecular Spectroscopy* **2003**, *59*, 957–962.

(31) Mohn, J.; Guggenheim, C.; Tuzson, B.; Vollmer, M. K.; Toyoda, S.; Yoshida, N.; Emmenegger, L. *Atmospheric Measurement Techniques* **2010**, *3*, 609–618.

(32) Mohn, J.; Tuzson, B.; Manninen, A.; Yoshida, N.; Toyoda, S.; Brand, W. A.; Emmenegger, L. *Atmospheric Measurement Techniques* **2012**, *5*, 1601–1609.

(33) Köster, J. R.; Well, R.; Tuzson, B.; Bol, R.; Dittert, K.; Giesemann, A.; Emmenegger, L.; Manninen, A.; Cárdenas, L.; Mohn, J. *Rapid communications in mass spectrometry : RCM* **2013**, *27*, 216–22.

(34) Miller, B. R.; Weiss, R. F.; Salameh, P. K.; Tanhua, T.; Greally, B. R.; Simmonds, P. G.; Mühle, J. *Analytical Chemistry* **2008**, *80*, 1536–1545.

(35) Potter, K. E.; Ono, S.; Prinn, R. G. *Rapid communications in mass spectrometry : RCM* **2013**, *27*, 1723–38.

(36) Potter, K. Nitrous oxide (N2O) isotopic composition in the troposphere: instrumentation, observations at Mace Head, Ireland, and regional modeling. PhD Thesis, Massachusetts Institute of Technology, 2011.

(37) Sirignano, C.; Neubert, R. E. M.; Rödenbeck, C.; Meijer, H. a. J. *Atmospheric Chemistry and Physics* **2010**, *10*, 1599–1615.

(38) Derwent, R.; Ryall, D.; Manning, A.; Simmonds, P.; O'Doherty, S.; Biraud, S.; Ciais, P.; Ramonet, M.; Jennings, S. *Atmospheric Environment* **2002**, *36*, 2799–2807.

(39) McManus, J. B.; Nelson, D. D.; Shorter, J.; Zahniser, M.; Mueller, A.; Bonetti, Y.; Beck, M.; Hofstetter, D.; Faist, J. *Proceedings of SPIE* **2002**, *4817*, 22–33.

(40) Rothman, L. et al. *Journal of Quantitative Spectroscopy and Radiative Transfer* **2009**, *110*, 533–572.

(41) Rothman, L. S.; Gamache, R. R.; Goldman, A.; Brown, L. R.; Toth, R. a.; Pickett, H. M.; Poynter, R. L.; Flaud, J. M.; Camy-Peyret, C.; Barbe, A.; Husson, N.; Rinsland, C. P.; Smith, M. a. *Applied Optics* **1987**, *26*, 4058–97.

(42) Nemtchinov, V.; Sun, C.; Varanasi, P. *Journal of Quantitative Spectroscopy and Radiative Transfer* **2004**, *83*, 267–284.

(43) Toth, R. A. *Journal of Quantitative Spectroscopy and Radiative Transfer* **2000**, *66*, 285–304.

(44) Lacome, N.; Levy, A.; Guelachvili, G. *Applied optics* **1984**, *23*, 425–35.

(45) Demtroeder, W. *Laser Spectroscopy: Basic Prin*, 4th ed.; Springer-Verlag: Berlin, Heidelberg, 2008; p 473.

(46) Tasinato, N.; Duxbury, G.; Langford, N.; Hay, K. G. *The Journal of chemical physics* **2010**, *132*, 044316.

(47) Kaiser, J.; Rockmann, T.; Brenninkmeijer, C. A. M.; Crutzen, P. J. *Atmospheric Chemistry and Physics* **2003**, *3*, 303–313.

(48) Bertolini, T.; Rubino, M.; Lubritto, C.; D'Onofrio, A.; Marzaioli, F.; Passariello, I.; Terrasi, F. *Journal of Mass Spectrometry* **2005**, *40*, 1104–8.

(49) Archbold, M. E.; Redeker, K. R.; Davis, S.; Elliot, T.; Kalin, R. M. *Rapid communications in mass spectrometry* **2005**, *19*, 337–42.

Supplementary Information: Development of a spectroscopic technique for continuous online monitoring of oxygen and site-specific nitrogen isotopic composition of atmospheric nitrous oxide

Eliza Harris,* David D. Nelson, William Olsewski, Mark Zahniser, Katherine E. Potter, Barry J. McManus, Andrew Whitehill, Ronald G. Prinn, and Shuhei Ono

E-mail: eliza.harris@empa.ch

*To whom correspondence should be addressed

1 Preconcentration of N_2O

The preconcentration unit is controlled with LabVIEW (National Instruments Corporation, USA). Zero air for the system is produced with a Parker Balston Zero Air Generator (model HPZA-3500) and dried with a Fluid Pro 50 membrane drier (Pentair Ltd.). The sample gas is passed through a Nafion drier (100 tubes, 48 inch, Perma Pure) prior to the trap to dry to a dew point of $<$-40°C to prevent the trap clogging with frozen water. The cryo-trap (T1 in Figure 1 of the main article) is made of a stainless steel tube (1/8" outer diameter, 0.085" ID) coiled on to an aluminium stand-off which is attached to a copper plate cooled by a Cryotiger Cold Head and a Polycold Compact Cooler (Brooks Automation, Inc.). The cooler has very low power requirements and has operated reliably in Medusa systems as a number of AGAGE stations for many years.[1] The trapping material is 27 cm (0.7 g) of 100-120 mesh glass beads (W.R. Grace & Co.) held in place with a glass wool plug and fine stainless steel mesh at each end.

During a trapping cycle, 0.2 - 0.4 L min^{-1} of sample gas is passed through the trap for 200-400 seconds. Trapping begins when the trap temperature drops below -156°C; the temperature is maintained at -156$\pm$2°C during trapping, as shown in Figure 2 of the main article. The trapping flow is regulated with mass flow controller (MFC) 1, and a pressure differential for the flow is maintained with diaphragm pump (DP) 1. The sample inlet pressure is maintained at 3 bar with DP 3 for a total pressure differential of 4 bar across MFC 1. DP 4 maintains a higher flow rate of $\sim$15 litres min^{-1} to ensure short residence time in the long inlet tubing to the tower. Following trapping, the trap is flushed with zero air and pumped out through the cell to remove non-condensibles and CO. The trap is isolated before being resistively heated to 30°C; the sample (primarily N_2O and CO_2) is then flushed into the cell with 4.4 sccm of zero air for 90 seconds, to give a pressure of $\sim$10 mbar in the cell. Then the position of valve 3 is changed, and the trap is cleaned by heating to 60°C, flushing with zero air, and pumping with DP 1, before the next sample is trapped. The laser absorption cell is pumped out with the scroll pump and pressurized with zero air to 40-50 mbar twice between each sample and standard analysis, as shown in Figure 2 of the main article.

2 Spectroscopic measurement of isotope ratios with TILDAS

2.1 Spectroscopic data acquisition

A TILDAS instrument (Aerodyne Research Inc.) was used for spectroscopic measurements.[2–4] The use of similar instrumentation for N_2O isotopomer measurements has been described previously,[5,6] however, the Stheno II TILDAS is unique in having two Peltier-cooled continuous-emission quantum cascade lasers (Alpes Lasers). 'Laser 1' is tuned to 2188 cm^{-1} for measurement of $^{14}N^{15}N^{16}O$ (456; $^{15}N^{\alpha}$), $^{15}N^{14}N^{16}O$ (546;$^{15}N^{\beta}$) and $^{14}N^{14}N^{16}O$ (446), and 'Laser 2' to 2203 cm^{-1} for measurement of $^{14}N^{14}N^{18}O$ (448) (see Figure 3 of the main article and Figure S1). The data quality is highest for the largest available peak of each species, therefore the $^{14}N^{15}N^{16}O$, $^{15}N^{14}N^{16}O$ and $^{14}N^{14}N^{16}O$ peaks in the 2203 cm^{-1} spectrum are included in the fit but not used for measurement.

The temperature of the laser system is controlled with a thermoelectric chiller (Thermocube, Solid State Cooling Systems, USA). Light is detected with a photovoltaic mercury cadmium telluride detector (Teledyne Judson Technologies, Series J19TE) also equipped with a thermoelectric cooler. Absorption spectra are measured for 400 and 350 points for Laser 1 and Laser 2, respectively, which is followed by the measurement of dark (no light) signal for 80 points. The lasers scan over these points for 6 msec (ie. at 1.54 kHz), and signal is averaged for one second. The concentrations of the species of interest are determined by fitting the measured one-second average spectrum to the modelled absorption by the isotopocules of N_2O, CO and CO_2 using a Voigt profile for the molecular line shape and a Gaussian approximation of the laser line width,[7] as shown in Figure 3 and Figure S1. The goodness of fit is estimated by comparing the fit to the measurement to calculate a χ^2 value. The typical value of χ^2 is a point-by-point standard deviation of 1×10^{-4} absorbance units. Data are rejected when the χ^2 of the fits is $> 5\times$ larger than the typical value, because the precision and accuracy of measurements is strongly reduced when the fit is poor. A background spectrum is taken with the cell under vacuum before every standard analysis, and the measured spectrum is obtained by dividing the raw spectrum by the background spectrum.

Spectrum fitting is performed with a frequency of 1 Hz.

2.2 Isotopic reference gases

Four different standard gas cylinders are used:

- Standard industrial compressed air (CA, Figure 1) is used to test the overall performance of the instrument. This standard is preconcentrated and analyzed in the same manner as ambient air samples, as described in the previous subsection. The precision of the isotopic measurements made for compressed air therefore provide a measure of the short- and long-term precision of preconcentrated measurements.

In addition, three reference gases are introduced to the absorption cell by simple gas expansion (Ref I, II and III) via a bulk expansion manifold, as shown in Figure 1 of the main article.

- Ref I and II are pure N_2O tanks (Air Gas, Inc., USA) maintained as secondary standards for long-term calibration. The isotopic compositions of Ref I and Ref II were externally verified by S. Toyoda at Tokyo Institute of Technology to correspond to the temporary calibration accepted by the research community in the absence of a true primary standard scale (Table S1).

- Ref III is a 65 ppm N_2O tank (Air Products, UK) used constantly as a tertiary working standard. The isotopic composition of Ref III was calibrated against Ref I and Ref II, so that Ref I and Ref II can be conserved to maintain a long-term standard scale.

For measurement, these three standard gases are mixed to have the same matrix composition as preconcentrated samples, to minimise the effects of pressure correction (discussed in Section S2.4): 65 ppm N_2O and 8% CO_2 in zero air.

Pressure regulators are used to set the pressure inside the standard reservoir (shown in Figure 1 of the main article) to $\sim$750 mbar to give a cell pressure of 10 mbar upon expansion. The reservoirs are opened to the standard tanks and then to the cell for $>$90 seconds to allow equilibration and

prevent isotopic fractionation. Ref III is run between every trapped sample peak as a reference gas, to account for laboratory temperature and laser conditions. The volume of the cell is approximately 685 mL, therefore <7 mL of standard is used per analysis ($< 0.5\mu$L of pure N_2O). The 50 L, 200 bar tank of Ref III would therefore suffice for >100 years of measurements (while the pure N_2O Ref I and Ref II tanks are used at a negligible rate) ensuring long-term traceability of the calibration scale. It is possible that the isotopic composition of Ref III will drift with time. The system has two standard reservoirs, so that Ref I and Ref II can be periodically run parallel to Ref III to account for longterm drift in the Ref III tank, to correct measurements to the international isotope standard scales of atmospheric N_2 for nitrogen isotopes and V-SMOW (Vienna Standard Mean Ocean Water) for oxygen isotopes.

2.3 Spectroscopic data analysis

Following measurement of raw concentrations of the different isotopomers with TILDAS (as described in Section 2 of the main article and Section S2.1), the data is analysed and corrected for background, matrix effects, and calibration to the international isotopic standard scale. A measurement consists of repeated standard-sample cycles. Each sample peak is ∼5 minutes long and each standard peak is ∼4 minutes long (see Figure 2 of the main article and Figure S2). The first minute of each peak is not used for isotopic analysis to ensure the measurement is not affected by the gas entering the cell; the last minute is also rejected as a buffer to ensure the 'peak' identified in the automatic data analysis does not overlap with the time when the sample is exiting the cell. The measured isotopic composition does not show detectable variation against time for the centre 2-3 minutes of the peak, thus the isotopic composition is averaged over this time (pale blue in Figure S2).

Background correction

The 'background' in the cell is measured between 0.8 and 0.2 minutes before the gas enters the cell, ie. after the cell has been cleaned by pressurization with zero air and then pumped out

to <0.9 mbar, shown in pale red in Figure S2. The pressure is 0.3 mbar higher in the background preceeding sample analyses due to the zero air flushing regime for the trap, however the N_2O mixing ratio is still >1000 times lower than during analysis. The sample and standard isotopic compositions are corrected for the background isotopic composition:

$$R_{456,\text{bcgcorr}} = \frac{R_{456,\text{raw}} \times [446]_{\text{raw}} - R_{456,\text{bcg}} \times [446]_{\text{bcg}}}{[446]_{\text{raw}} - [446]_{\text{bcg}}} \quad (1)$$

where R_{456} is $\frac{[^{14}N^{15}N^{16}O]}{[^{14}N^{14}N^{16}O]}$ averaged across the peak or the background (and analogously for $^{15}N^{14}N^{16}O$ and $^{14}N^{14}N^{18}O$). Average values for the correction are shown in Table S1. The background correction is on average slightly negative (∼-0.03‰), showing that the background is isotopically heavy compared to the samples and standards. This is expected given the lighter isotopocules will diffuse faster and be preferentially pumped out of the cell.

Calibration to international isotopic standard scale

The samples are calibrated to V-SMOW and atmospheric N_2 scales for oxygen and nitrogen isotopic composition respectively using the measured values of the reference gas Ref III (see Section S2.2). A reference gas 'correction factor' is calculated from the measured isotope ratio of Ref III as: $\text{CF}_{456} = \frac{R_{456,\text{known}}}{R_{456,\text{bcgcorr}}}$ and analogously for $^{15}N^{14}N^{16}O$ and $^{14}N^{14}N^{18}O$. The correction factors are smoothed as a running average of three, to account for random error in the standard measurements, and interpolated to the point of each sample analysis, as shown in Figure S2d. The correction factors drift slowly with temperature and laser conditions by less than 0.1‰ hour^{-1} (see Table S1), thus results are accurate as long as conditions are stable over a few hours. Table S1 shows the exceptional stability of the system, with medium-term drifts (days to weeks) on the order of 0.1 ‰ or less. Delta values for samples are then found by:

$$\delta_{456,\text{stdcorr}}(‰) = [(R_{456,\text{bcgcorr}} \times \text{CF}_{456}) - 1] \times 1000 \quad (2)$$

where $\delta_{456} \equiv \delta^{15}N^{\alpha}$ and analogously for $^{15}N^{14}N^{16}O$ and $^{14}N^{14}N^{18}O$.

The average correction factor is -1.1% (CF = 0.989), -2.5% (0.975), and +3.3% (1.033) for 456, 546 and 448, respectively, as shown in Table S1. The primary contributor to the correction factors is uncertainty in the absorption line strength and broadening coefficients compiled in the HITRAN database,[8,9] which are only accurate to around 3 to 4%.[10,11] Correction factors are typically stable to within 0.1‰ over three measurement cycles; those differing from the running mean by more than 0.6‰ are rejected as outliers. There are almost no correction factors varying from the mean by 0.3-0.6‰ (∼3-6 standard deviations); outliers are clearly distinguished and occur approximately once every 40 standard analyses (<once per day).

Matrix correction

Measured isotopologue ratios are sensitive to the matrix, particularly the CO_2 partial pressure, and the total bath gas pressure. Therefore, a pressure correction is applied based on the difference in matrix composition (CO, CO_2 and bath gas pressure) between the sample and the average composition of the standards used to calculate the CF values:

$$\begin{aligned}\delta_{456,\text{final}} = \delta_{456,\text{stdcorr}} + (\text{P}_{\text{CO,std}} - \text{P}_{\text{CO,sam}}) \times \text{PCF}_{\text{CO,456}} + \\ (\text{P}_{\text{CO}_2,\text{std}} - \text{P}_{\text{CO}_2,\text{sam}}) \times \text{PCF}_{\text{CO}_2,456} + (\text{P}_{\text{bath,std}} - \text{P}_{\text{bath,sam}}) \times \text{PCF}_{\text{bath,456}}\end{aligned} \quad (3)$$

where P is the pressure of CO, CO_2 or bath gas in mbar for the standards or the sample and PCF is the pressure correction factor in ‰ mbar^{-1} (see Table S1 and Section S2.4). PCFs for $\delta^{15}\text{N}^{\alpha}$ and $\delta^{15}\text{N}^{\beta}$ in terms of CO pressure are negligibly different from 0 ‰ mbar^{-1} due to the small size of the CO peak in Laser 1. CO_2 and bath gas pressures are matched as closely as possible between samples and standards to minimize the pressure corrections, however, ambient CO_2 mixing ratios show large variation. The error in pressure correction factors is <5% as the relationships are very linear and well-defined across the range of matrix composition encountered in typical ambient measurements (see Figure S3). The average bath gas pressure correction is ∼1‰ (Table S1) introducing an error of <0.05‰, while the error introduced by changing CO_2 pressure in ambient samples is <0.025‰.

Measurement precision

The accuracy of the technique and the uncertainty in the results is defined as the standard deviation of repeated analyses of compressed air, which occur every 5-10 samples, to account for the reproducibility of trapping and matrix conditions in the cell.

2.4 Effect of matrix components on measured isotopic composition

The composition of the matrix plays a critical role in the accuracy of the measurements due to the effects on peak shape and width, discussed further in Sections 3.1.1 and S4. Preconcentrated samples ($\sim$1200 mL of ambient air) consist of $\sim$65 ppm N_2O and $\sim$8% CO_2, with zero air flush added to bring the pressure to 10 mbar. Standards are mixed to match this matrix composition as closely as possible, although manually-mixed standards can have compositions varying by 20-30%. The measurement conditions were chosen as a compromise between the advantage of narrow peaks with minimal baseline overlap at low pressure and low concentrations, and the need for sufficiently large peaks for accurate fitting.

The main matrix gas is zero air. Some 'air' component may remain on the trap, altering the N_2:O_2 ratio of the trapped samples relative to the standards. This could potentially alter peak shapes and thus measured isotopic ratio, leading to random or systematic errors in measurements. Therefore, the peak shapes and measured isotopic composition with varying N_2:O_2 ratio were investigated. The four major N_2O peaks measured with 100% N_2, 100% O_2 and the normal air bath gas are shown in Figure S4. The deviation between the peak shapes is $<$2%. The O_2 matrix peaks may be slightly broader than the other peaks, however the difference is not significant. The measured isotopic compositions of Ref II mixed in three different bath gas mixtures are presented in Figure 4 and Table S4. The results confirm that the N_2:O_2 composition of the matrix has no significant effect on isotopic measurements.

Previous use of preconcentration with TILDAS isotope measurement has involved CO_2 removal,[6,12,13] however chemical CO_2 traps such as Ascarite need to be replaced often, which is

not ideal for deployment at remote stations. Use of chemical traps also risks the possibility of unwanted chemical reactions with the sample gas. The pressure of CO_2 in the cell affects the measured isotopic composition of N_2O by $\sim$3 to 4 ‰ per mbar of CO_2 partial pressure (Figure S3 and Table S1). The bath gas pressure affects the measured N_2O isotopic composition with the same order of magnitude as the CO_2 pressure. These effects are caused by small changes in peak shapes due to the different broadening and narrowing effects of these gases (Sections 3.1.1 and S4), which affect the baseline and the fit. The pressure of bath gas can be keep constant to $\pm$2% by controlling the flush into the cell, however the ambient CO_2 mixing ratio, and thus the in-cell CO_2 mixing ratio, will vary by $>$10% at Mace Head Station.[14,15]

When the sample and the standard have different matrix compositions, the isotopic composition of the sample is not accurate because the 'correction factor' (CF, see Section S2.3) measured for the standard is not exactly applicable to the sample conditions. Therefore, a pressure correction is applied (PCF, Section S2.3). The total magnitude of the correction is $<$2‰ (Table S1 and Figure S2e). The pressure correction factors are determined empirically every two weeks by measuring a standard and adding spikes of matrix gases and determining a fit as shown in Figure S3; the factors are very linear and change less than 5% over longer time periods. As shown in Figure 4 of the main article, the measured isotopic composition for the 14% CO_2 sample in TILDAS agrees very well with the pure N_2O measurement of the same sample with IR MS. Relative to the standard, the 14% CO_2 sample has a 0.64 mbar difference in CO_2 pressure in the cell, resulting in corrections of -1.73$\pm$0.09‰, 1.67$\pm$0.08‰ and -2.56$\pm$0.13‰ for $\delta^{15}N^{\alpha}$, $\delta^{15}N^{\beta}$ and $\delta^{18}O$ respectively. 14% CO_2 would correspond to approximately 700 ppm CO_2 in atmosphere for an ambient preconcentrated sample, thus normal ambient variation in CO_2 mixing ratio will not significantly affect measurement accuracy.

3 Synthesis of standards by ammonium nitrate decomposition

To compare isotopic measurements by IR MS and TILDAS over a wide range of site-specific isotopic compositions, N_2O gases were synthesised by ammonium nitrate decomposition.[16–18] Five different N_2O isotopic standards were made (summarised in Table S2). For ^{15}N-enriched N_2O, (TROP-A, TROP-B and ENR), pure NH_4NO_3 and ^{15}N spiked-NH_4Cl or $NaNO_3$ (Sigma Aldrich) as specified in Table S2 were dissolved in 15 mL of water at 100°C in a hot water bath. The solution was cooled to 0°C in an ice bath to form NH_4NO_3 crystals and the remaining solution was decanted off. This was repeated and before drying the crystals overnight at 80°C.

To prepare isotopically-depleted NH_4NO_3 (DEP) from $^{14}NH_4Cl$ and $Na^{14}NO_3$ a large quantity of the isotopic spike is required, so excess Cl^- and Na^+ must be removed before recrystallisation, or these salts will reform preferentially before NH_4NO_3 will precipitate. Therefore, 1 g of $Na^{14}NO_3$ was dissolved in 10 mL of MilliQ water and run through Dowex 50WX8 (50-100 mesh, H^+ form) ion exchange resin twice. This resin has a strong affinity for Na^+ compared to H^+, thus H^+ is released while Na^+ is retained by the resin. The initial pH of the solution was 7; following elution the pH had dropped to 0.5. 1 g of $^{14}NH_4Cl$ was added to the $H^{14}NO_3$ solution (from $Na^{14}NO_3$ cation exchange; 10 mL at 1.2 mol L^{-1}) and K_2CO_3 was added until the pH reached 10 ($\sim$1 g); the jar was then kept capped to minimise loss of $^{14}NH_3$ gas. The solution was cooled to 0°C in an ice bath to precipitate KCl, which was removed by filtration (Whatman ashless filter paper circles). 1 g of NH_4NO_3 was dissolved in the remaining solution. The volume was reduced by leaving overnight at 50°C and the NH_4NO_3 was recrystallised and dried.

NH_4NO_3 enriched in $\delta^{18}O$ was produced by mixing 1 mL of HNO_3 (69% reagent grade, Sigma Aldrich) with 1 mL of ^{18}O-enriched water (97% ^{18}O, Cambridge Isotope Laboratories). The solution was left at 90°C for 75 hours to allow oxygen isotope exchange between nitrate and water.[19,20] 1 mL of NH_4OH (27%) and 1 g of NH_4NO_3 was then dissolved in the solution. The volume was reduced by leaving overnight at 50°C and the NH_4NO_3 was recrystallised and dried.

Between 70-80 mg of NH_4NO_3 was weighed into $\sim$30 cm lengths of glass tube (3/8" outer diameter, 1/4" inner diameter, medium wall, Chemglass) and flame-sealed under vacuum. NH_4NO_3

was decomposed by slowly heating to 270°C over 190 minutes, holding at 270°C for 10 hours, and cooling to room temperature over 190 minutes.[21] The resultant N_2O was purified and collected on the manifold shown in Figure S5. The glass tubes were attached to the 'tube cracker', and the system was pumped out before the tube was cracked to release N_2O. Repeated distillations were performed between the two cold fingers, with an ethanol-dry ice slurry (-80°C) to remove water, and liquid nitrogen to collect N_2O, before pumping out non-condensibles. Finally, the purified N_2O was expanded into a flask and mixed with bulk N_2O (Ref II; $\delta^{15}N^{\alpha}$ = -0.78‰, $\delta^{15}N^{\beta}$ = 0.3‰, $\delta^{18}O$ = 40.43‰) to achieve a array of isotopic compositions covering the range expected in the present-day troposphere; dilution factors are shown in Table S2.

Ideally, N_2O decomposition would preceed according to:

$$NH_4NO_3 \rightarrow N_2O + 2\,H_2O \tag{4}$$

Some water was therefore present from the desired decomposition reaction, while non-condensibles, primarily N_2, can be formed by side reactions.[22] The average pressure of non-condensibles on the first distillation was 60-130 mbar; following the third distillation non-condensibles were below the manometer detection limit (0.1 mbar). Example gas chromatographs of product purity are shown in Figure S6; the N_2O in all cases had no detectable CO_2, which could impact the accuracy of IR MS analyses.[23] The yield of the decomposition was between 70-90%. Some lost yield would be due to side reactions, but the majority of lost yield is expected to be due to human error during transfer of the NH_4NO_3 into the glass tubes and partial decomposition of some grains (those sticking to the tube sides) during the flame-sealing. Some isotopic fractionation may occur during possible side reactions, however loss during transfer and decomposition of those grains stuck on the walls are expected to be bulk processes and introduce no isotopic fractionation.

4 Spectroscopic line shapes and pressure broadening effects

The Lorentz width can be approximated as a linear combination of broadening due to air, self (N_2O) and CO_2 *:

$$\Delta\nu_L = \gamma_{\text{air}} \times \text{P}_{\text{air}} + \gamma_{\text{self}} \times \text{P}_{\text{self}} + \gamma_{\text{CO2}} \times \text{P}_{\text{CO2}} \tag{5}$$

where $\Delta\nu_L$ is the peak width (HWHM in cm^{-1}), γ_{air}, γ_{self} and γ_{CO2} are the pressure-broadening coefficients (in cm^{-1} atm^{-1}) in air, for self-broadening, and in CO_2 respectively, and P is the pressure (in atm) of each matrix component. The pressure of N_2O is more than three orders of magnitude less than the pressure of CO_2 therefore self-broadening of N_2O lines can be ignored. To separate the broadening effects of CO_2 and air, the partial pressures of these two matrix components were varied separately. The pressure-broadening coefficients can then be found from the slope of the Lorentz width with the pressure of the broadening gas (Figure S7).

The Doppler width, which narrows with pressure due to the Dicke narrowing effect,[24,25] was approximated by:

$$\Delta\nu_D = \Delta\nu_{D0}(1 - \beta_{\text{CO2}} \times \text{P}_{\text{CO2}} - \beta_{\text{air}} \times \text{P}_{\text{air}}) \tag{6}$$

where $\Delta\nu_D$ is the peak width with pressure and $\Delta\nu_{D0}$ is the Doppler peak width at 0 atm pressure, and β_{CO2} and β_{air} are the Dicke narrowing factors in CO_2 and air. This can be rearranged assuming that the pressure of CO_2 is constant to find the Dicke narrowing factor for air:

$$\beta_{\text{air}} = \frac{1}{\partial P_{CO2}} + \frac{\partial(\Delta\nu_D)}{\partial P_{air}} \frac{1}{\Delta\nu_{D0}} \tag{7}$$

and similarly assuming that the pressure of air is constant to find the Dicke narrowing factor for CO_2. The values of β_{CO2} and β_{air} can therefore be estimated from this parameterisation using the slope and intercept of the Doppler width with pressure of air and CO_2 (Figure S7). The results are discussed in Section 3.1.1 of the main article.

*Pressure is in units of atmospheres (atm) in this section for consistency with the HITRAN database.

5 Scrambling correction in the IR MS

Scrambling factor corrections have been described previously in a number of papers (such as Toyoda et al. 1999,[17] Kaiser et al. 2003,[26] and Westley et al. 2007[22]). The details of the equations and the terminology varies slightly between different studies, therefore the exact equations used in the current study are given here for clarity (following Westley et al., 2007[22]):

5.1 One factor scrambling correction

The one factor scrambling correction assumes that the yield of ^{15}NO from ^{15}NNO is equal to the yield of ^{14}NO from $N^{15}NO$, and that further isotope substitutions do not affect scrambling. To calculate the final isotopic composition (adapted from[22])[†]:

1. $N_2\,^{18}O^+$ is assumed to be the only contributor to mass 46:

$$R_{18} = \frac{m_{46}}{m_{44}} \tag{8}$$

2. Mass dependent oxygen isotopic composition is assumed:

$$R_{17} = R_{17,\mathrm{V-SMOW}} \cdot \left(\frac{R_{18}}{R_{18,\mathrm{V-SMOW}}}\right)^{0.516} \tag{9}$$

where $R_{X,\mathrm{V-SMOW}}$ is the isotopic composition of Vienna Standard Mean Ocean Water

3. R_{15^β} is estimated by assuming $^{14}N^{15}N^{16}O$ and $^{15}N^{14}N^{16}O$ contribute equally to mass 45:

$$R_{15^\beta} = \left(\frac{m_{45}}{m_{44}} - R_{17}\right)/2 \tag{10}$$

[†] $R_{18} = \frac{[^{14}N^{14}N^{18}O]}{[^{14}N^{14}N^{16}O]}$, $R_{17} = \frac{[^{14}N^{14}N^{17}O]}{[^{14}N^{14}N^{16}O]}$, $R_{15^\alpha} = \frac{[^{14}N^{15}N^{16}O]}{[^{14}N^{14}N^{16}O]}$ and $R_{15^\beta} = \frac{[^{15}N^{14}N^{16}O]}{[^{14}N^{14}N^{16}O]}$

4. Mass 31 is solved to find R_{15^α} using the scrambling factor γ:

$$R_{15^\alpha} = (\frac{m_{31}}{m_{30}} - R_{17} - \gamma.R_{15^\beta})/(1-\gamma) \tag{11}$$

5. R_{18} is recalculated to account for clumped isotopocule contributions:

$$R_{18} = \frac{m_{46}}{m_{44}} \; - \; (R_{15^\alpha} + R_{15^\beta}).R_{17} \; - \; R_{15^\alpha}.R_{15^\beta} \tag{12}$$

6. Step 2 is repeated to recalculate R_{17}

7. R_{15^β} is recalculated to include account for the actual value of R_{15^α}:

$$R_{15^\beta} = \frac{m_{45}}{m_{44}} - R_{17} - R_{15^\alpha} \tag{13}$$

8. Steps 4 through 7 are repeated for twenty iterations to find the final isotopic composition of the sample

5.2 Two factor scrambling correction

The two factor scrambling correction accounts for differences between the yield of ^{15}NO from ^{15}NNO (γ_β) and the yield of ^{14}NO from N^{15}NO (γ_α), however, further isotope substitutions do not affect scrambling. A six factor scrambling model which accounts for all isotopic differences is described in,[22] however the number of measurements made in this study is insufficient to assess the accuracy of this model. To calculate the final isotopic composition with two scrambling factors (adapted from[22]):

1. $N_2\,{}^{18}O^+$ is assumed to be the only contributor to mass 46:

$$R_{18} = \frac{m_{46}}{m_{44}} \tag{14}$$

2. Mass dependent oxygen isotopic composition is assumed:

$$R_{17} = R_{17,\mathrm{V-SMOW}} \cdot \left(\frac{R_{18}}{R_{18,\mathrm{V-SMOW}}}\right)^{0.516} \tag{15}$$

where $R_{X,\mathrm{V-SMOW}}$ is the isotopic composition of Vienna Standard Mean Ocean Water

3. R_{15^β} is estimated by assuming $^{14}N^{15}N^{16}O$ and $^{15}N^{14}N^{16}O$ contribute equally to mass 45:

$$R_{15^\beta} = \left(\frac{m_{45}}{m_{44}} - R_{17}\right)/2 \tag{16}$$

4. Mass 31 is solved to find R_{15^α} using the two scrambling factors, γ_α and γ_β:

$$R_{15^\alpha} = \frac{\frac{m_{31}}{m_{30}}.(1+(1-\gamma_\beta).R_{15^\beta}) \; - \; \gamma_\beta.R_{15^\beta} \; - \; R_{17}.(1+(1-\gamma_\beta).R_{15^\beta})}{1 \; + \; R_{15^\beta} \; - \; \gamma_\alpha.(1-R_{17}+\frac{m_{31}}{m_{30}})} \tag{17}$$

5. R_{18} is recalculated to account for clumped isotopocule contributions:

$$R_{18} = \frac{m_{46}}{m_{44}} \; - \; (R_{15^\alpha}+R_{15^\beta}).R_{17} \; - \; R_{15^\alpha}.R_{15^\beta} \tag{18}$$

6. Step 2 is repeated to recalculate R_{17}

7. R_{15^β} is recalculated to include account for the actual value of R_{15^α}:

$$R_{15^\beta} = \frac{m_{45}}{m_{44}} - R_{17} - R_{15^\alpha} \tag{19}$$

8. Steps 4 through 7 are repeated for twenty iterations to find the final isotopic composition of the sample

6 Figures S1-S10 and Tables S1-S5

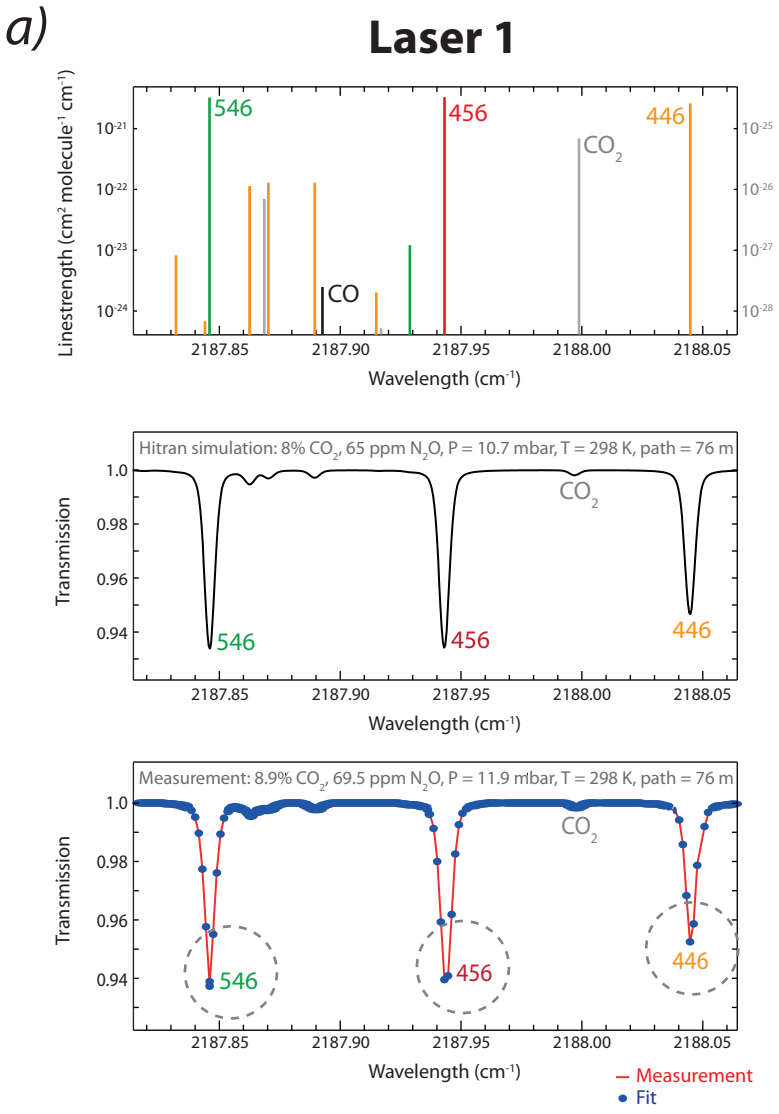

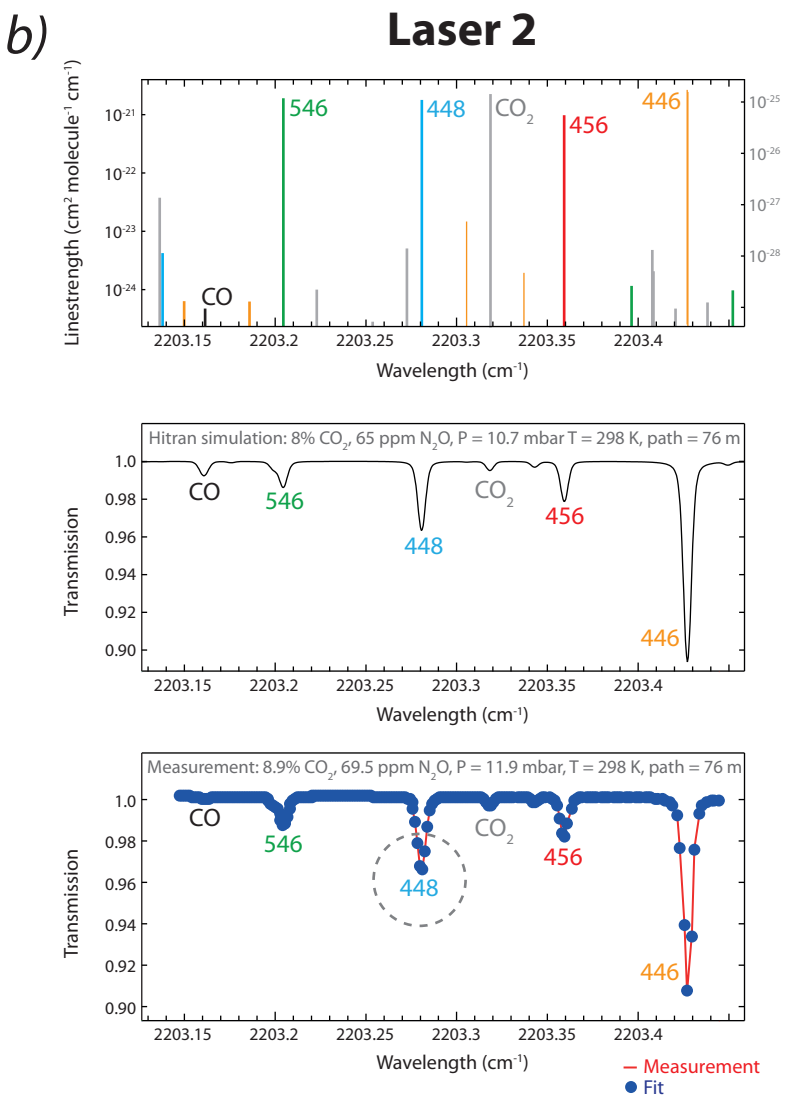

278 **Figure S1.** Absorption lines for N_2O, CO_2 and CO for *a*) Laser 1: 2188 cm^{-1} and *b*) Laser
279 2: 2203 cm^{-1}. Top panels: absorption lines from HITRAN database. Middle panels: simulated
280 spectrum of a typical sample, accounting for pathlength, concentration, pressure and temperature.
281 Bottom panels: Measured (blue dots) and fit (red line) spectrum used for measurement of N_2O
282 isotopic composition. The peaks used for isotope measurements are indicated with a gray dashed
283 circle.

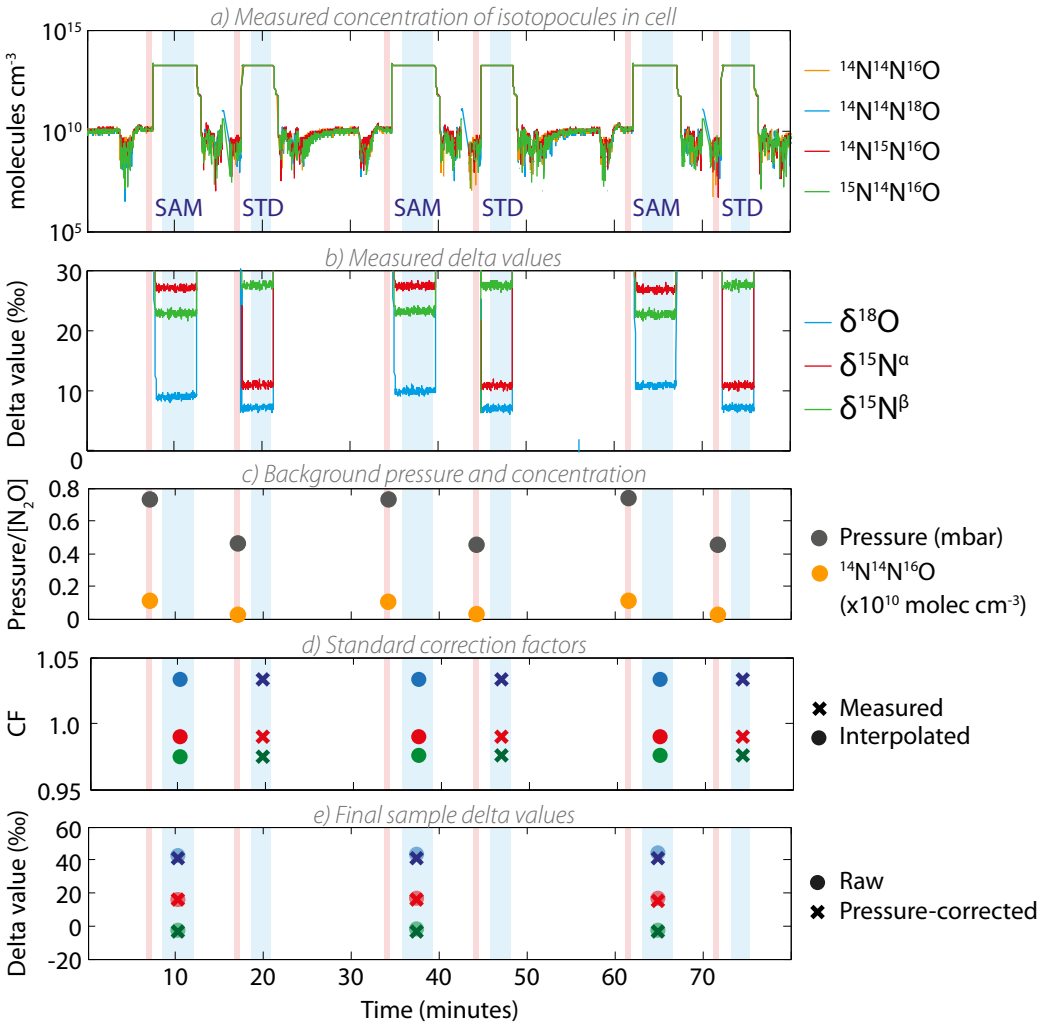

Figure S2. Data analysis procedure for TILDAS measurements of N_2O isotopic composition: a) Running concentrations of N_2O isotopocules normalised to $^{14}N^{14}N^{16}O$ concentration to facilitate visualisation, b) Running measurements of δ-values when sample or standard is in the cell (not shown when samples are not in the cell as error makes the values not meaningful), c) Pressure and N_2O ($^{14}N^{14}N^{16}O$) concentration of the background, immediately before the sample or standard gas enters the cell, d) Measured and interpolated standard correction factors (ie. $\delta_{known}/\delta_{measured}$) and e) final standard δ values, raw and corrected for matrix differences between samples and standards. In all panels, colour-coding is the same: $^{14}N^{14}N^{18}O$ = blue, $^{14}N^{15}N^{16}O$ = red and $^{15}N^{14}N^{16}O$ = green. Error bars are smaller than points and therefore not shown.

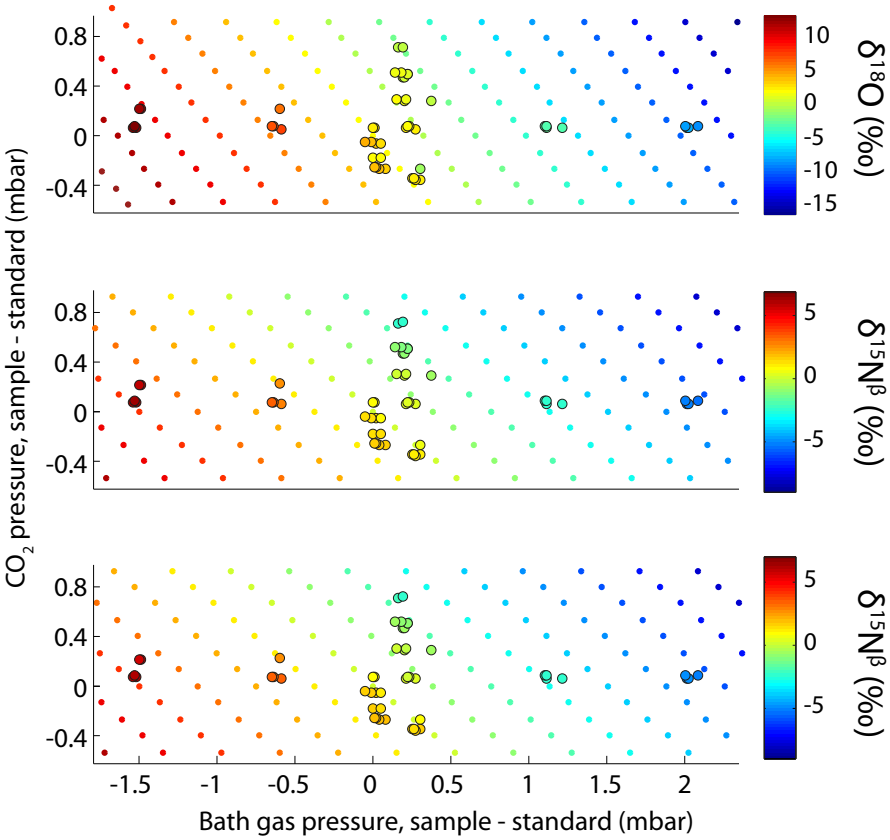

293 **Figure S3.** Effect of bath gas and CO_2 pressure on measured isotopic composition of N_2O.
294 Large points with black borders show measured deviation of isotopic composition from the true
295 value due to changes in the matrix (‰, color bar on right hand side). Small points show the fit to
296 the data that is used to correct measurements.

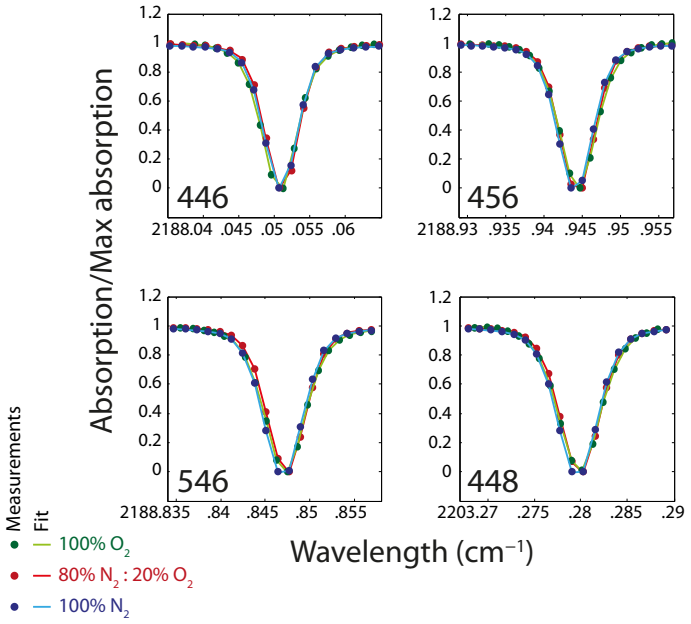

Figure S4. Line shapes of the major N_2O peaks at a mixing ratio of ∼65 ppm with 8% CO_2 and 0.01 atm bath gas: 100% O_2 (green), 80% N_2 and 20% O_2 (air, red) and 100% N_2 (blue). Absorption is shown relative to the maximum absorption to normalise the effect of small variations in N_2O mixing ratio between the three measurements.

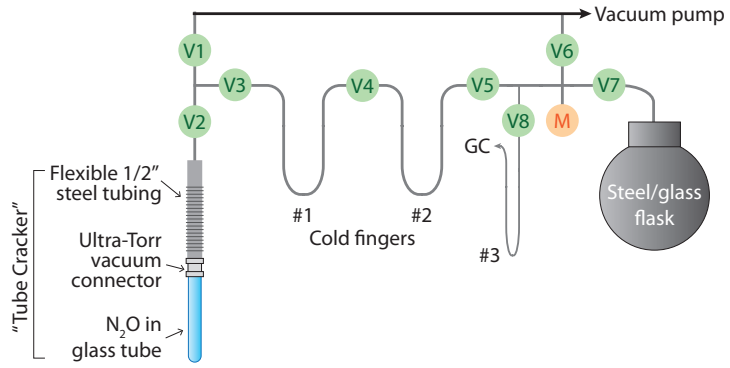

Figure S5. Vacuum manifold used for the purification of N_2O synthesised by the decomposition of NH_4NO_3. V = valve, M = manometer, GC = gas chromatograph.

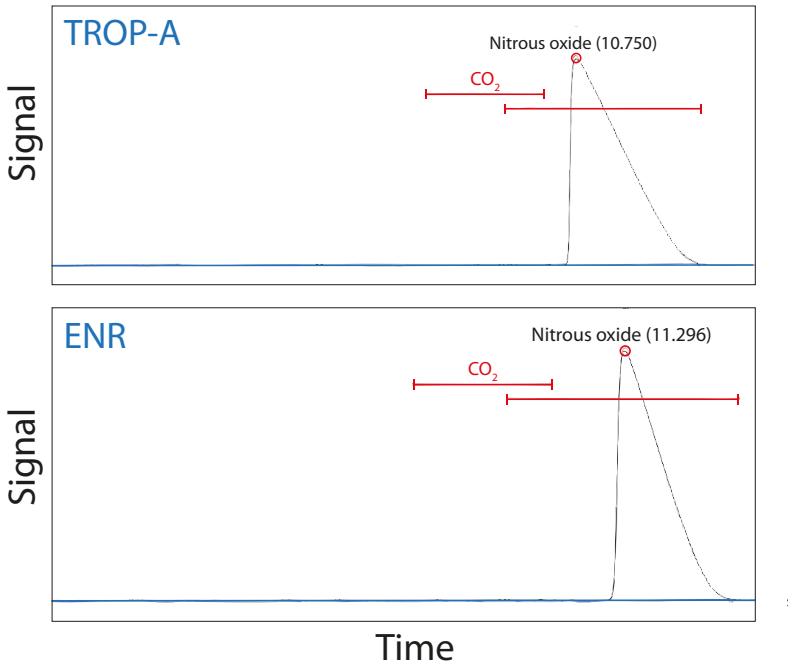

Figure S6. Gas chromatograph measurements of N_2O formed for the decomposition of NH_4NO_3 and purified by distillation with ethanol-dry ice slurry and liquid nitrogen. Retention time windows for CO_2 and N_2O are shown in red; the exact retention time is shown in brackets following the peak identity.

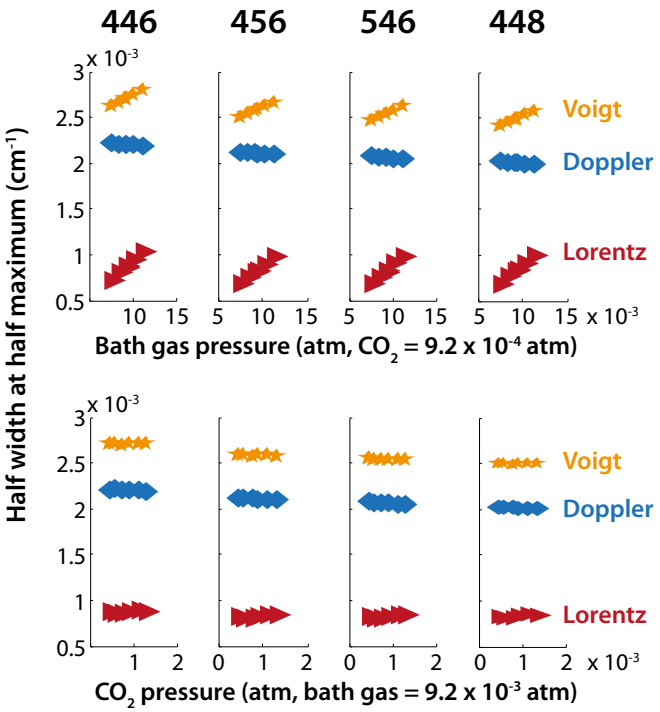

310 **Figure S7.** Peak width changes attributed to Doppler profile: Dicke narrowing (blue) and
311 Lorentz profile: pressure broadening (red) and Voigt profile: total width (yellow) for N_2O peaks
312 with changes in bath gas (zero air) pressure (top panels) and CO_2 pressure (lower panels).

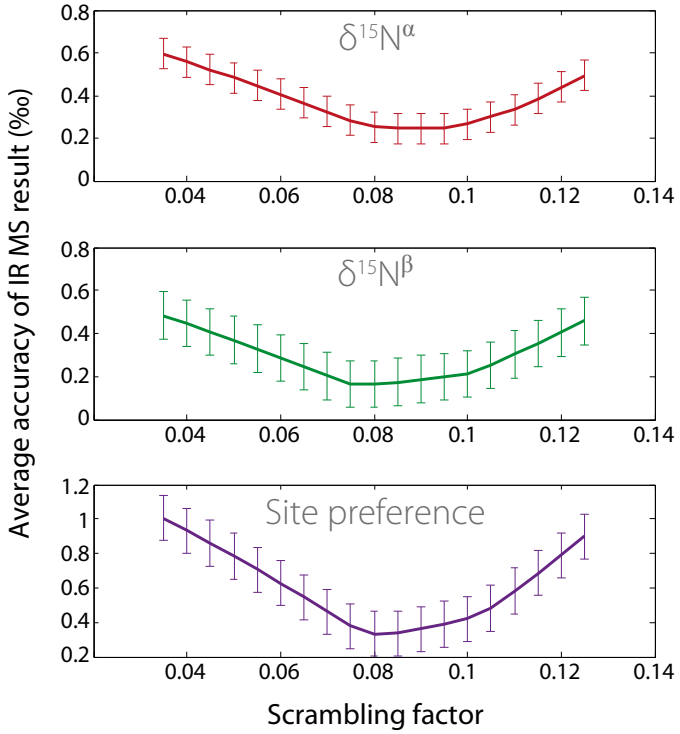

313 **Figure S8.** Absolute accuracy of site-specific N_2O isotopic measurements made with IR MS
314 using a one factor scrambling model (defined as $|\,(\delta^{15}N^{\alpha})_{\mathrm{IRMS}} - (\delta^{15}N^{\alpha})_{\mathrm{TILDAS}}\,|$ averaged across
315 the six N_2O standards, and similarly for $\delta^{15}N^{\beta}$ and site preference). Error bars are the 1σ standard
316 deviation.

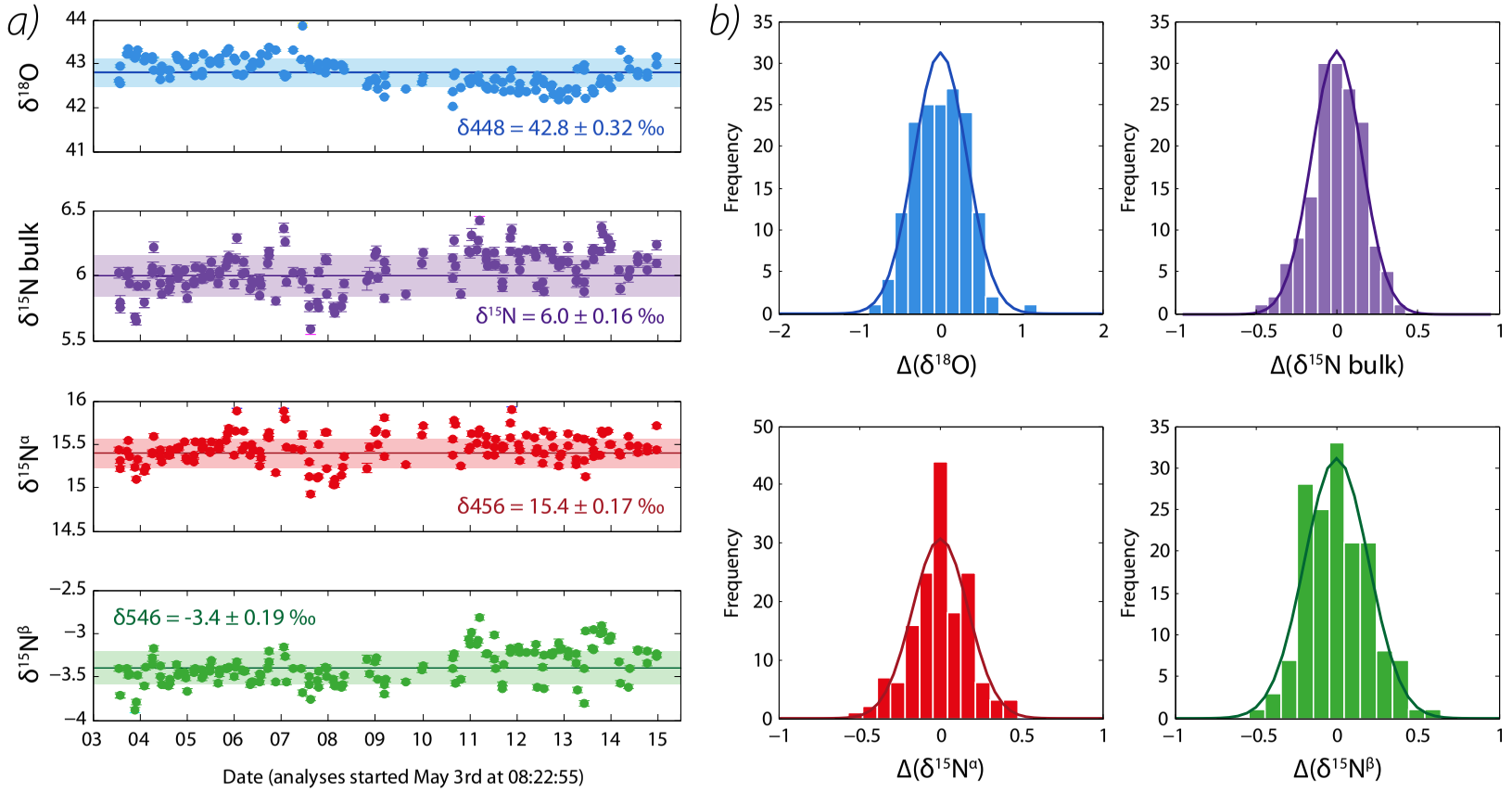

Figure S9. N_2O isotope ratios from repeated measurements of compressed air. *a*) Measured isotopic composition with time. Error bars are the 1σ standard deviation from repeated 1 second measurements during the ~100 seconds the sample is in the cell. *b*) Frequency distribution of deviations from the mean value in permil; ie. $\Delta(\delta^{18}O) = \delta^{18}O_x$ - mean($\delta^{18}O$). Bars show the measured frequency (bins are σ/2 wide) and lines show the fit to a Gaussian distribution.

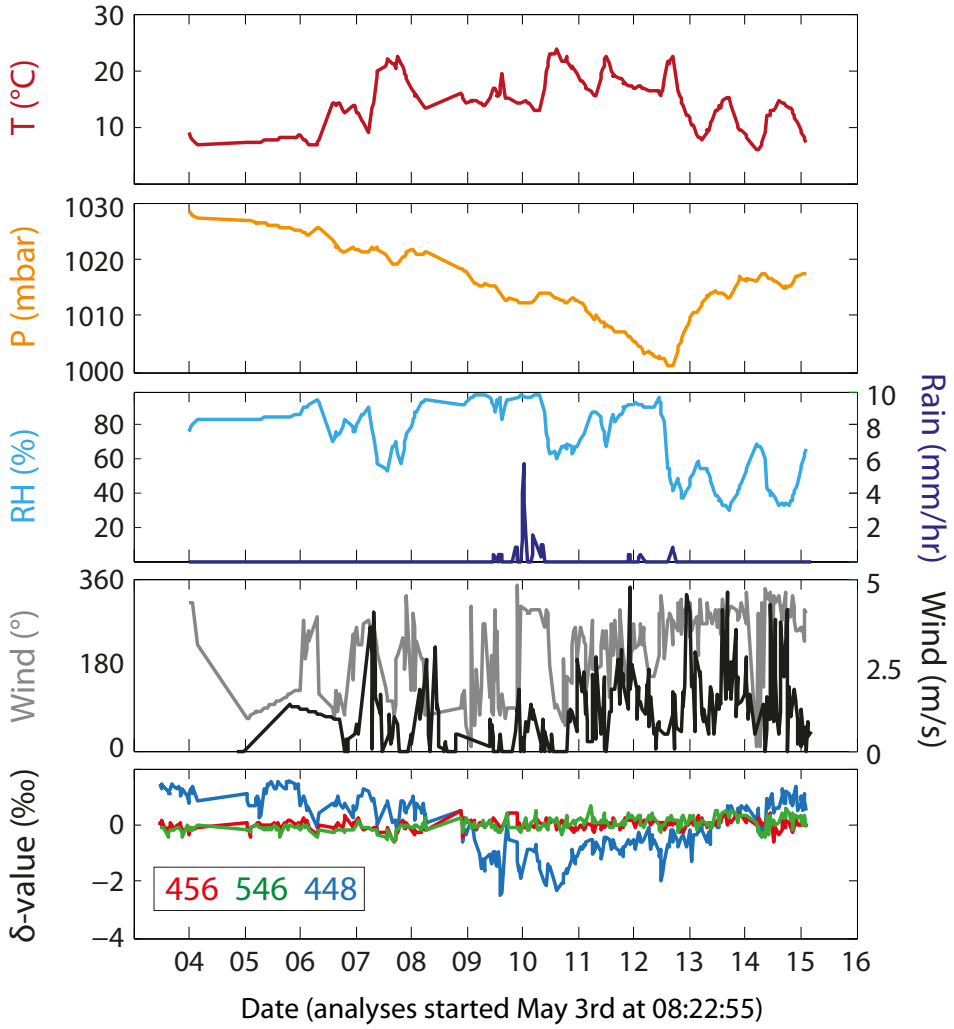

Figure S10. Meteorological data during the measurement period. T = temperature in °C. P = pressure in mbar. RH = relative humidity in %. Rain = precipitation per hour. Wind = wind direction in degrees and wind speed in m/s. δ-value = normalised isotopic composition: 456 in red, 546 in green and 448 in blue. Meterological data from Weather Underground.[?]

	$\delta^{15}N^{\alpha}$	$\delta^{15}N^{\beta}$	$\delta^{18}O$
Background correction			
Mean background pressure (mbar), standard		0.39±0.02	
Mean background pressure (mbar), trapped samples		0.91±0.03	
Mean correction (‰)	-0.025	-0.024	-0.034
Correction against standards			
Mean correction (‰)	-10.70	-25.13	-33.13
Mean difference between points[a] (‰)	0.096	0.078	0.088
Short-term drift[b] (‰ $hour^{-1}$)	0.08	0.1	0.088
Long-term drift[c] (‰ day^{-1})	0.08	0.04	0.009
Pressure correction			
Mean bath gas pressure (mbar), standard		9.882±0.004	
Mean bath gas pressure (mbar), sample		9.52±0.03	
Bath gas pressure dependence (‰ $mbar^{-1}$)	-2.6	-2.6	-6.0
Mean CO_2 pressure (mbar), standard		0.8482±0.0006	
Mean CO_2 pressure (mbar), sample		0.906±0.004	
CO_2 pressure dependence (‰ $mbar^{-1}$)	-2.7	-2.6	-4.0
Mean CO pressure (mbar), standard		$(2.33\pm0.03)\text{x}10^{-7}$	
Mean CO pressure (mbar), sample		$(1.28\pm0.02)\text{x}10^{-4}$	
CO pressure dependence[d] (‰ $mbar^{-1}$)	∼0	∼0	-0.17

Table S1. Corrections applied to raw TILDAS data to account for N_2O background in the cell, calibration to international isotopic standard scale, and pressure dependence of isotopic measurements. Pressure dependencies are found from slopes of measured δ values with varying matrix, as shown in Figure S3, and are accurate to <5%. [a]Average difference between adjacent standard correction factors. [b]Short-term drift is on the order of hours and is primarily due to changes in laboratory temperature throughout the day. [c]Long-term drift is the change in mean correction factor per day on average over the entire measurement period of 13 days. [d]CO dependence is negligible for $\delta^{15}N^{\alpha}$ and $\delta^{15}N^{\beta}$ as the CO peak on Laser 1 is very weak.

Table S2. N_2O isotope standards synthesised by ammonium nitrate decomposition. Methods are described in detail in Section S3. Dilution refers to mixing of the N_2O from decomposition with bulk N_2O. All isotopically-labelled compounds are from Sigma Aldrich.

Name	Method	Components	Dilution
TROP-A	Simple recrystallisation	15 g stock NH_4NO_3 + 10 mg $Na^{15}NO_3$	1:10
TROP-B	Simple recrystallisation	∼15 g stock NH_4NO_3 + ∼10 mg $Na^{15}NO_3$ + ∼0.5 mg $^{15}NH_4Cl$	1:10
ENR	Simple recrystallisation	∼15 g stock NH_4NO_3 + ∼20 mg $Na^{15}NO_3$ + ∼10 mg $^{15}NH_4Cl$	1:10
DEP	1. $Na^{15}NO_3$ through cation resin to remove Na^+ 2. Add $^{1}4NH^{4}Cl$ and K_2CO_3 to precipitate Cl^- 3. Add stock NH_4NO_3 and recrystallise	∼1 g stock NH_4NO_3 + ∼1 g $Na^{15}NO_3$ + ∼1 g $^{15}NH_4Cl$	1:10
448-H	1. Equilibrate $H_2^{18}O$ with HNO_3 2. Add NH_4OH and stock NH_4NO_3 and recrystallise	∼1 g stock NH_4NO_3 + ∼1 mL 69% HNO_3 + 1 mL 27% NH_4OH	1:130

Table S3. Measurement conditions for IR-MS analyses of N_2O isotopic composition. 'Emission' is the current heating the cathode of the ion source. 'Trap' is the voltage of the electron trap, which is held at a positive potential relative to the ionization chamber. 'Extraction' is a percentage value related to the potential of the extraction plates used to accelerate ions of the ionization chamber; a larger number corresponds to a lower potential difference between the ionization chamber and the extraction plates.[27]

Fragment	N_2O^+	NO^+
Masses	44, 45, 46, 47	30, 31, 32, 33
Emission	1.5 mA	1.5 mA
Trap	4.9 V	4.9 V
Electron Energy	95.079	95.079
Extraction	27.08%	17.53

Table S4. N_2O reference gas measurements comparing the accuracy of measurements made with isotope ratio-mass spectrometry (IR-MS) and quantum cascade laser spectroscopy (QCL). 'Matrix' is the gas composition in the QCL cell; a normal matrix is 65 ppm N_2O, 8% CO_2 in zero air bath gas at 0.010 atm pressure. Errors are the 1σ standard deviation of multiple measurements for both techniques. [a]Calibrated at the Tokyo Institute of Technology (TITech) by S. Toyoda as $\delta^{18}O = 40.14 \pm 0.10$ ‰, $\delta^{15}N_\alpha = -0.44 \pm 0.02$ ‰ and $\delta^{15}N_\beta = 1.50 \pm 0.06$ ‰. [b]Calibrated at TITech as $\delta^{18}O = 40.43 \pm 0.04$ ‰, $\delta^{15}N_\alpha = -0.78 \pm 0.04$ ‰ and $\delta^{15}N_\beta = 0.30 \pm 0.04$ ‰.[21]

		$\delta^{18}O$		$\delta^{15}N^\alpha$		$\delta^{15}N^\beta$	
	QCL matrix	**IR-MS**	**QCL**	**IR-MS**	**QCL**	**IR-MS**	**QCL**
Ref I[a]	Normal	40.26±0.14	40.39±0.14	-0.51±0.05	-0.16±0.12	1.44±0.07	1.61±0.10
Ref II[b]	Normal	40.41±0.14	40.35±0.33	-0.71±0.05	-0.46±0.09	0.43±0.07	0.38±0.11
	N_2 bath gas		40.60±0.20		-0.72±0.09		0.12±0.09
	O_2 bath gas		40.73±0.54		-0.60±0.48		-0.74±0.42
	14% CO_2		40.16±0.12		-0.20±0.09		0.40±0.15
TROP-A	Normal	39.83±0.14	40.42±0.07	19.07±0.05	18.92±0.05	4.91±0.07	5.22±0.10
	40.5 ppm N_2O		38.29±0.13		18.37±0.14		3.41±0.28
TROP-B	Normal	40.07±0.14	40.35±0.05	17.08±0.05	16.80±0.06	4.49±0.07	4.76±0.13
	23.5 ppm N_2O		38.11±0.12		16.70±0.11		-0.58±0.35
	244 ppm N_2O		39.67±0.26		16.26±0.25		4.78±0.14
ENR	Normal	39.88±0.14	40.04±0.12	28.54±0.05	28.78±0.11	29.97±0.07	29.71±0.14
DEP	Normal	38.59±0.14	38.06±0.08	-21.11±0.05	-20.71±0.08	-35.44±0.07	-35.80±0.07
448-H	Normal	148.70±0.14	149.86±0.25	-6.96±0.05	-1.39±0.19	-0.23±0.07	0.24±0.20

	T	**P**	**RH**	**Rain**	**WD**	**WS**
	°	mbar	%	mm/hr	degrees	m/s
Mean	13.9	1016	73.6	0.1	204	1.1
Variability (1σ)	4.6	6.8	20.2	0.5	85.3	1.0
$\delta^{18}O$	**0.34**	**0.46**	**0.05**	**0.05**	<0.01	<0.01
$\delta^{15}N^{\alpha}$	0.02	**0.04**	<0.01	<0.01	<0.01	<0.01
$\delta^{15}N^{\beta}$	<0.01	**0.17**	**0.12**	0.02	**0.09**	<0.01
$\delta^{15}N_{bulk}$	<0.01	**0.14**	**0.07**	<0.01	**0.05**	<0.01

Table S5. R^2 values showing the fraction of variability in isotopic composition predicted by six different weather variables: temperature (T), pressure (P), relative humidity (RH), precipitation (Rain), wind direction (WD) and wind speed (WS). Significant correlations are highlighted in bold (two-tailed *t*-test, $p<0.02$, n = 302). The mean value and 1σ standard deviation for each variable is also given.

References

(1) Miller, B. R.; Weiss, R. F.; Salameh, P. K.; Tanhua, T.; Greally, B. R.; Simmonds, P. G.; Mühle, J. Medusa : A Sample Preconcentration and GC / MS Detector System for in Situ Measurements of Atmospheric Trace Halocarbons , Hydrocarbons , and Sulfur Compounds. *Analytical Chemistry* **2008**, *80*, 1536–1545.

(2) Nelson, D. D.; McManus, B.; Urbanski, S.; Herndon, S.; Zahniser, M. S. High precision measurements of atmospheric nitrous oxide and methane using thermoelectrically cooled mid-infrared quantum cascade lasers and detectors. *Spectrochimica Acta Part A* **2004**, *60*, 3325–35.

(3) McManus, J. B.; Zahniser, M. S.; Nelson, D. D.; Williams, L. R.; Kolb, C. E. Infrared laser spectrometer with balanced absorption for measurement of isotopic ratios of carbon gases. *Spectrochimica Acta Part A* **2002**, *58*, 2465–79.

(4) McManus, J. B. Application of quantum cascade lasers to high-precision atmospheric trace gas measurements. *Optical Engineering* **2010**, *49*, 111124.

(5) Wächter, H.; Mohn, J.; Tuzson, B.; Emmenegger, L.; Sigrist, M. W. Determination of N2O isotopomers with quantum cascade laser based absorption spectroscopy. *Optics Express* **2008**, *16*, 9239–9244.

(6) Mohn, J.; Tuzson, B.; Manninen, A.; Yoshida, N.; Toyoda, S.; Brand, W. A.; Emmenegger, L. Site selective real-time measurements of atmospheric N2O isotopomers by laser spectroscopy. *Atmospheric Measurement Techniques* **2012**, *5*, 1601–1609.

(7) McManus, J. B.; Nelson, D. D.; Shorter, J.; Zahniser, M.; Mueller, A.; Bonetti, Y.; Beck, M.; Hofstetter, D.; Faist, J. Quantum cascade lasers for open and closed path measurement of atmospheric trace gases. *Proceedings of SPIE* **2002**, *4817*, 22–33.

(8) Rothman, L. et al. The HITRAN2012 molecular spectroscopic database. *Journal of Quantitative Spectroscopy and Radiative Transfer* **2013**,

(9) Rothman, L. S.; Gamache, R. R.; Goldman, A.; Brown, L. R.; Toth, R. a.; Pickett, H. M.; Poynter, R. L.; Flaud, J. M.; Camy-Peyret, C.; Barbe, A.; Husson, N.; Rinsland, C. P.; Smith, M. a. The HITRAN database: 1986 edition. *Applied Optics* **1987**, *26*, 4058–97.

(10) Toth, R. A. N2- and air-broadened linewidths and frequency-shifts of N2O. *Journal of Quantitative Spectroscopy and Radiative Transfer* **2000**, *66*, 285–304.

(11) Rothman, L. et al. The HITRAN 2004 molecular spectroscopic database. *Journal of Quantitative Spectroscopy and Radiative Transfer* **2005**, *96*, 139–204.

(12) Mohn, J.; Guggenheim, C.; Tuzson, B.; Vollmer, M. K.; Toyoda, S.; Yoshida, N.; Emmenegger, L. A liquid nitrogen-free preconcentration unit for measurements of ambient N2O isotopomers by QCLAS. *Atmospheric Measurement Techniques* **2010**, *3*, 609–618.

(13) Köster, J. R.; Well, R.; Tuzson, B.; Bol, R.; Dittert, K.; Giesemann, A.; Emmenegger, L.; Manninen, A.; Cárdenas, L.; Mohn, J. Novel laser spectroscopic technique for continuous analysis of N2O isotopomers–application and intercomparison with isotope ratio mass spectrometry. *Rapid communications in mass spectrometry : RCM* **2013**, *27*, 216–22.

(14) Sirignano, C.; Neubert, R. E. M.; Rödenbeck, C.; Meijer, H. a. J. Atmospheric oxygen and carbon dioxide observations from two European coastal stations 2000-2005: continental influence, trend changes and APO climatology. *Atmospheric Chemistry and Physics* **2010**, *10*, 1599–1615.

(15) Derwent, R.; Ryall, D.; Manning, A.; Simmonds, P.; O'Doherty, S.; Biraud, S.; Ciais, P.; Ramonet, M.; Jennings, S. Continuous observations of carbon dioxide at Mace Head, Ireland from 1995 to 1999 and its net European ecosystem exchange. *Atmospheric Environment* **2002**, *36*, 2799–2807.

(16) Friedman, L.; Bigeleisen, J. Oxygen and Nitrogen Isotope Effects in the Decomposition of Ammonium Nitrate. *The Journal of Chemical Physics* **1950**, *18*, 1325.

(17) Toyoda, S.; Yoshida, N. Determination of nitrogen isotopomers of nitrous oxide on a modified isotope ratio mass spectrometer. *Analytical Chemistry* **1999**, *71*, 4711–4718.

(18) Brenninkmeijer, C. A. M.; Röckmann, T. Mass spectrometry of the intramolecular nitrogen isotope distribution of environmental nitrous oxide using fragment-ion analysis. *Rapid Communications in Mass Spectrometry* **1999**, *13*, 2028–2033.

(19) Bohlke, J. K.; Mroczkowski, S. J.; Coplen, T. B. Oxygen isotopes in nitrate: new reference materials for O-18 : O-17 : O-16 measurements and observations on nitrate-water equilibration. *Rapid Communications In Mass Spectrometry* **2003**, *17*, 1835–1846.

(20) Kool, D. M.; Wrage, N.; Oenema, O.; Van Kessel, C.; Van Groenigen, J. W. Oxygen exchange with water alters the oxygen isotopic signature of nitrate in soil ecosystems. *Soil Biology and Biochemistry* **2011**, *43*, 1180–1185.

(21) Potter, K. Nitrous oxide (N2O) isotopic composition in the troposphere: instrumentation, observations at Mace Head, Ireland, and regional modeling. PhD Thesis, Massachusetts Institute of Technology, 2011.

(22) Westley, M.; Popp, B. N.; Rust, T. M. The calibration of the intramolecular nitrogen isotope distribution in nitrous oxide measured by isotope ratio mass spectrometry. *Rapid Communications in Mass Spectrometry* **2007**, *21*, 391–405.

(23) Kaiser, J.; Röckmann, T.; Brenninkmeijer, C. A. M. Complete and accurate mass spectrometric isotope analysis of tropospheric nitrous oxide. *Journal of Geophysical Research* **2003**, *108*, 4476–.

(24) Rao, D. R.; Oka, T. Dicke narrowing and pressure broadening in the infrared fundamental band of HCl perturbed by Ar. *Journal of Molecular Spectroscopy* **1987**, *122*, 16–27.

(25) Tasinato, N.; Duxbury, G.; Langford, N.; Hay, K. G. An investigation of collisional processes in a Dicke narrowed transition of water vapor in the 7.8 microm spectral region by frequency down-chirped quantum cascade laser spectroscopy. *The Journal of chemical physics* **2010**, *132*, 044316.

(26) Kaiser, J.; Rockmann, T.; Brenninkmeijer, C. A. M.; Crutzen, P. J. Wavelength dependence of isotope fractionation in N2O photolysis. *Atmospheric Chemistry and Physics* **2003**, *3*, 303–313.

(27) ThermoFinnigan, *MAT 253 Operating Manual*; 2002; p 78.